UNIVERSITÀ DEGLI STUDI DI MILANO

CORSO DI DOTTORATO IN BIOLOGIA MOLECOLARE E CELLULARE

XXXVI Ciclo

DIPARTIMENTO DI BIOSCIENZE

TESI DI DOTTORATO DI RICERCA

UNDERSTANDING THE PRO-SURVIVAL ROLE OF AIF: STRUCTURAL AND FUNCTIONAL STUDY OF AIF-CHCHD4 COMPLEX

Elisa FAGNANI
R13026

Tutor: Prof. Alessandro ALIVERTI
Co-tutor: Dr. Mario MILANI

Coordinatore del dottorato: Prof. Roberto MANTOVANI

A.A. 2022-2023

Contents

Part II

Manuscripts under revision

1) *CHCHD4 binding affects the active site of apoptosis inducing factor (AIF): structural determinants of the allosteric regulation.* Structure Journal.

2) *Stabilization of the retromer complex: analysis of novel binding sites of bis-1,3-phenyl guanylhydrazone 2a to the VPS29/VPS35 interface.* Computational and Structural Biotechnology Journal.

Abstract

Apoptosis Inducing Factor (AIF), a highly conserved mitochondrial flavoprotein, is generally known as a caspase-independent effector in the intrinsic apoptosis pathway. Beside this apoptotic function, recent studies demonstrate that AIF is also able to regulate the cell energy homeostasis by promoting the biogenesis and the function of multi-subunit respiratory complexes. Although the underlying molecular mechanisms have not been yet elucidated, it is clear that this role is played thanks to the interaction of AIF with CHCHD4, a soluble inter membrane space (IMS) protein which promotes the entrance in the IMS and the oxidative folding of substrates belonging to the respiratory complexes' subunits. Given the interest in deeply understanding the AIF vital role in mitochondria, we decided to investigate the AIF-CHCHD4 interaction from both the functional and the structural point of view. We focused on the study of the possible impact of the 27-residues N-terminal portion of CHCHD4, which effectively mimics the protein binding site with AIF, on the catalytic activity and NAD^+-binding ability of AIF. The peptide turned out to stimulate the DCIP-NADH reductase activity of AIF, allowing the estimation of the apparent K_d of the AIF-peptide complex in the sub-micromolar range. Another interesting finding was the ability of AIF to bind NAD^+ only in the presence of peptide. The experiments indicate that NAD^+ complexation is strongly stimulated by lowering the temperature and that such effect is secondary to the AIF-peptide interaction. The same effect was obtained even with the full length form of CHCHD4. Another important feature observed is that CHCHD4 or its peptide binding also modulates the AIF reactivity towards thiol-containing compounds revealing a possible role of AIF in assisting the oxidative folding of disulfide-containing polypeptides in mitochondria. The interaction between AIF and CHCHD4 was then further investigated through

different biophysical techniques such as analytic Size Exclusion Chromatography (SEC), ThermoFAD, Microscale Thermophoresis and Isothermal Titration Calorimetry. In particular, we found out that AIF and CHCHD4 form a heterodimeric complex, whose stability is temperature-dependent, with a binding affinity in the low micromolar range for oxidised AIF and in the low nanomolar range for reduced AIF. For the determination of relevant structural features of the complex, we used AlphaFold software to build up a model, which was then experimentally confirmed by mass-spectrometry analyses on the cross-linked AIF-CHCHD4 complex. Since peptide and NAD^+ bindings display strong positive cooperativity, we used this information to set up the optimal conditions for X-ray diffraction studies, through which we determined the crystal structure of the complex. The binding site of AIF for CHCHD4 was further validated by mutagenesis experiments on AIF.

Riassunto

Il fattore di induzione dell'apoptosi (AIF), una flavoproteina mitocondriale altamente conservata, è generalmente noto per il suo ruolo nell'attivazione del processo di apoptosi intrinseca in maniera indipendente dalle caspasi. Oltre a questa funzione pro-apoptotica, studi recenti hanno dimostrato che AIF è anche in grado di regolare l'omeostasi energetica cellulare promuovendo la biogenesi e la funzione dei complessi respiratori multi-subunità. Sebbene i meccanismi molecolari alla base non siano stati ad oggi chiariti, è noto che questo ruolo è svolto grazie all'interazione di AIF con CHCHD4, una proteina solubile dello spazio inter-membrana dei mitocondri (IMS), che promuove l'ingresso nell'IMS e il *folding* ossidativo dei substrati appartenenti alle subunità dei complessi respiratori. Dato l'interesse nel chiarire il ruolo vitale di AIF nei mitocondri, abbiamo deciso di indagare l'interazione AIF-

CHCHD4 sia dal punto di vista funzionale che strutturale. Ci siamo concentrati sullo studio del possibile impatto della porzione N-terminale di CHCHD4 (27 residui), sufficiente per legare AIF, sull'attività catalitica di AIF e sulla sua capacità di legare il NAD^+. Si è scoperto che il peptide stimola l'attività DCIP-NADH reduttasica di AIF ed è stata stimata una K_d apparente del complesso AIF-peptide nel basso micromolare. Un'altra interessante scoperta è stata la capacità di AIF di legare NAD^+ solo in presenza del peptide. Gli esperimenti indicano che l'interazione con NAD^+ è fortemente stimolata dall'abbassamento della temperatura e che tale effetto è secondario all'interazione AIF-peptide. Lo stesso effetto è stato ottenuto anche con la forma intera di CHCHD4. Inoltre, è stato osservato che il legame di CHCHD4 o del suo peptide modula anche la reattività di AIF verso composti contenenti gruppi tiolici, suggerendo un possibile ruolo di AIF nell'assistere il *folding* ossidativo dei polipeptidi contenenti disolfuri all'interno dei mitocondri. L'interazione tra AIF e CHCHD4 è stata poi ulteriormente studiata attraverso diverse tecniche biofisiche come la cromatografia analitica ad esclusione molecolare, ThermoFAD, termoforesi e calorimetria. In particolare, abbiamo scoperto che AIF e CHCHD4 formano un complesso eterodimerico, la cui stabilità dipende dalla temperatura, con un'affinità di legame nel basso micromolare per AIF ossidata e nel basso nanomolare per AIF ridotta. Per la determinazione delle caratteristiche strutturali del complesso, abbiamo utilizzato il software AlphaFold per costruire un modello, che è stato poi confermato sperimentalmente da analisi di spettrometria di massa sul complesso AIF-CHCHD4 covalentemente legato. Poiché il legame del peptide e di NAD^+ mostrano una forte cooperatività positiva, abbiamo utilizzato queste informazioni per determinare le condizioni ottimali per gli studi di diffrazione a raggi X, attraverso i quali abbiamo determinato la struttura cristallografica del complesso. Il sito di legame di AIF per CHCHD4 è stato ulteriormente validato tramite esperimenti di mutagenesi su AIF.

1. Introduction

1.1 Flavoproteins

Flavoproteins represent a wide class of enzymes catalysing different redox activities through distinct chemical mechanisms. They perform several reactions such as dehydrogenation, oxidation and hydroxylation of metabolites and are involved in various cellular processes from DNA damage repair to light emission (1). Despite the large number of enzymatic activities related to flavoproteins, a common feature is represented by electrons transfer between the substrate and the flavin cofactor during the catalytic activity.

Flavoproteins contain two types of prosthetic groups: flavin adenine dinucleotide (FAD) and flavin mononucleotide (FMN). FAD and FMN contain a tricyclic heteroaromatic isoalloxazine ring able to accept or donate one/two electrons. They are synthetised from vitamin B2 (riboflavin) by riboflavin kinase and FAD-adenylyl transferase (2). Riboflavin was originally isolated in 1879, by Alexander Wynter Blyth, from a cow milk whey showing a particular yellow/green fluorescence once exposed to light and he firstly named it “lactochrome”. In 1933 Richard Kuhn isolated the coloured component from milk and subsequently confirmed the isoalloxazine derivative structure of the substance with two methyl groups and a sugar (pentose) radical attached, hence the name riboflavin. Few years later, Otto Heinrich Warburg and collaborators were studying biological oxidations involved in cellular respiration when they isolated, from brewer’s yeast, a “yellow enzyme”. Warburg noticed that after enzyme dialysis, both the colour and the enzymatic activity were lost and that the latter was re-established only in presence of both the apoprotein and the pigment. In 1935, Hugo Theorell confirmed this finding and demonstrated that the

yellow pigment was actually FMN (3). Only three years later, Warburg and Christian isolated and characterised the FAD prosthetic group of D-amino acid oxidase (4).

The redox-active part of flavin is constituted by the 7,8-dimethylisoalloxazine while the side chains, as the adenine part, are not directly involved in the catalytic functions but serve for coenzyme anchoring to the enzyme active site. Flavin reduction occurs through two possible mechanisms: two one-electron steps or one two-electrons step. In both the cases, the chemical changes involve atoms N(1), N(5) and C(4a). The redox potential of flavins is mainly influenced by its environment, indeed while positive charges increase the redox potential of pyrimidine, the presence of negative charges or hydrophobic surroundings decrease it. Another important factor affecting the potential of the redox-active part of flavin is the introduction of functional groups which modify the flavin nucleus. Anyway, the type of reactions involving flavins determines the specific locus at which the reaction of their nucleus with substrates occurs (1).

As anticipated, flavoproteins are involved in several processes inside the cells related to the wide range of catalytic activities performed. Therefore, many human disorders are associated to flavoprotein gene mutations and, since most of these proteins are located inside mitochondria, a considerable number of diseases are related to mitochondrial impairment. Other flavoproteins dysfunctions or deficiencies regard peroxisomes and the endoplasmic reticulum or are connected to metabolic pathways. Several studies report that many flavoenzymes are involved in the biogenesis of other cofactors, such as coenzymes A and Q, in the metabolism of different substrates as folate and cobalamin, and in the biosynthesis of cell signalling molecules like steroid and thyroid hormones (2).

Among mitochondrial flavoenzymes, the Apoptosis Inducing Factor (AIF) family represents a class of flavin-bound proteins implicated in oxido-reduction processes in the primary metabolism of the human body.

1.2 Apoptosis Inducing factor

1.2.1 Apoptosis inducing factor family

In 1999, Guido Kroemer discovered a mitochondrial enzyme able to induce apoptosis, also in isolated nuclei, in a caspase-independent manner and called this protein "apoptosis inducing factor" (AIF). He found out that AIF is able to induce the release of apoptogenic factors from mitochondria and to translocate itself into the nucleus causing chromatin condensation (5).

Apoptosis Inducing Factor family, in *Homo sapiens*, is composed of three main proteins that share the apoptogenic function, the physiological localization in mitochondria and the presence of FAD and NADH binding domains. The three proteins of the family are known as apoptosis-inducing factor mitochondrion-associated 1, 2 and 3; also named AIF, AMID (AIF-homologous mitochondrion-associated inducer of death) and AIFL (apoptosis-inducing factor-like), respectively. While AIF and AIFL have 27% of sequence identity, AMID shares a 19% sequence identity with the other two members of the family (6). The three AIFs present high similarities with bacterial and mammalian NADH-oxidoreductases, in particular with NADH dehydrogenases (NDH). NDH are mitochondrial enzymes which regulate the homeostasis of NAD(H) and are involved in apoptotic processes. Evolutionary studies confirmed the distinction of two phylogenetic branches: the AIF/AIFL branch and the AMID/NDH one. Further analyses demonstrated that AIFs have eubacterial origin

and that the sequence differences between the three AIFs and NDH occurred before eukaryotic divergence, also proven by domain architecture distinctions (7). Among the three proteins of the family, AIF is the most characterised member at molecular, biochemical and cellular level.

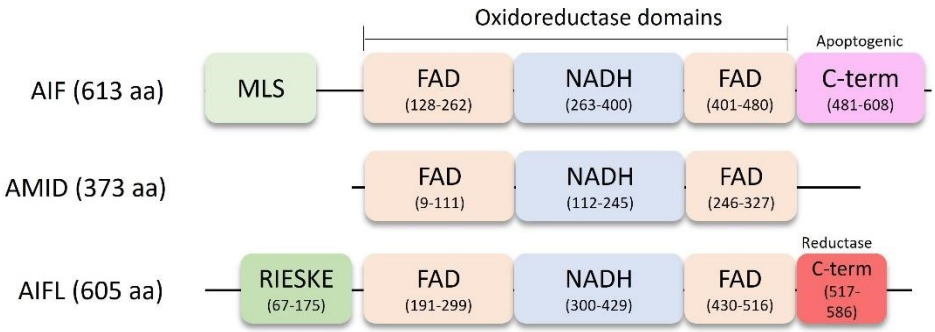

Fig.1.1 Scheme of domains in human AIF family members. Bipartite FAD-binding domain, NADH binding domain, C-terminal domain (apoptogenic in AIF, reductase in AIFL) and RIESKE domain are represented in orange, light blue, violet, red and green, respectively (with the residues included in each domain). Mitochondrial localization sequence (MLS) is in light green.

1.2.2 AIF gene and major protein forms

AIF is encoded by the *AIFM1* gene mapped on X-chromosome region A6 in mouse and region Xq25±26 in human. The primary translation product of the AIF gene is a precursor protein of about 67 KDa and 613 residues. The N-terminal portion of the protein, up to residue 53, represents a mitochondrial localization sequence (MLS) essential for AIF entrance inside mitochondria (5). Once inside the organelle, the

MLS is cleaved by mitochondrial peptidases and the protein reaches its mature fold (AIFΔ1-54) and integrates the FAD cofactor. AIFΔ1-54 then is anchored to the inner membrane of mitochondria (IMM) thanks to the presence of a trans-membrane sequence at the N-terminus.

The 96-120 segment of AIFΔ1-54 contains two proteolytic sites which, after an apoptotic stimulus, are cleaved by mitochondrial or cytoplasmic proteases, leading to the soluble form of AIF (57 KDa, AIFΔ1-102). Upon the permeabilization of the outer mitochondrial membrane cytosolic AIFΔ1-102 translocates to the nucleus thanks to the presence of two nuclear localization signals (NLS) located in the centre and in the C-terminal part of the protein, where executes apoptosis (8).

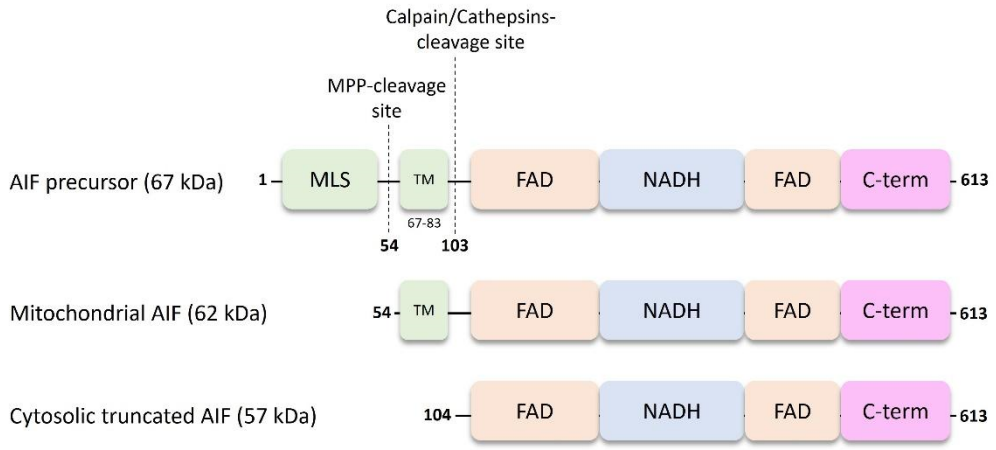

Fig. 1.2 Sequences of major human AIF forms. In AIF precursor (67 KDa) the MLS, the transmembrane region, the Mitochondrial Processing Peptidase (MPP) and calpain/cathepsin cleavage sites, the FAD and NADH -binding domain and C-terminal domain are reported. Mitochondrial AIF (62 KDa) is the mature form of the protein obtained after mitochondrial processing. Cytosolic AIF (57 KDa) is the apoptogenic form, released in the cytosol after apoptotic signals.

1.2.3 AIF structure

The re-folded murine AIFΔ1-120 was the first protein to be well characterised from both the biological and structural point of view (PDB: 1GV4) (9). Structure characterization revealed a glutathione-reductase (GR)-like fold and the binding of one FAD molecule (10). As a GR-like protein, AIF has three main domains: the FAD-binding domain (residues 122–262 and 400–477), the NADH-binding domain (residues 263–399) and a C-terminal domain (residues 478–610). The first two domains show the classical Rossmann topology characterised by the presence of six β strands forming an extended β sheet surrounded by α helices on both faces, producing a three-layered sandwich. The C-terminal domain, instead, displays five antiparallel β strands (residues 477–579) followed by two α helices (residues 580–610).

The FAD moiety non-covalently binds AIF in an elongated manner. More in details, while the adenine nucleoside and the pyrophosphate group of FAD binds the most conserved part of the FAD-binding domain (residues 138–140, 164, 232, 258–260 and 403), the isoalloxazine ring is partially exposed to the solvent suggesting its role as a redox centre (9). The FAD-binding domain represents the most conserved region in GR-like proteins, however, AIF shows a peculiarity regarding its N-terminal part (residues 190-202). This region, indeed, has a unique β hairpin fold which directly interacts with the protein core through hydrophobic (residues 190, 192 and 195) and polar residues (residues 194 and 200) (8). Concerning the NADH-binding domain, in GR-like proteins the nicotinamide-binding portion is more conserved than the adenine-binding one. With respect to the other members of the superfamily, AIF NADH-binding domain is characterised by the absence of hydrogen bonds both with the pyrophosphate group and the ribose moiety of NADH. This feature results in a larger pocket with weaker NADH interaction. The C-terminal domain of AIF is the

most peculiar protein portion. Compared to other GR-like proteins, AIF C-terminal domain displays a long 509-559 insertion folded in two short helices followed by an elongated Pro-rich loop. The loop also contains a PEST sequence, responsible for interactions with other proteins, and together with the mentioned β hairpin regulates the accessibility to the protein active site (9).

Considering that refolding significantly alters the redox properties of AIF, in 2009 Sevrioukova *et al.* solved the structure of naturally folded murine AIFΔ1-77 through X-ray crystallography with a resolution of 2.95 Å (PDB: 3GD3). This structure lacks the N-terminal transmembrane portion mimicking the mature AIFΔ1-53 both in function and structure (11). Like AIFΔ1-120, also AIFΔ1-77 is present as a dimer in the crystallographic lattice, even if both proteins in solution are monomeric. Comparing the two structures it was possible to identify some differences. The FAD moiety in the refolded protein shows a displacement of 0.5 Å for adenosine and a 0.7 Å one for isoalloxazine moiety. Moreover, the peptide 438-450, which in refolded AIF is an elongated loop, in the naturally folded protein is arranged in a β turn. This different conformation alters the position of Arg448 which, instead of forming a salt bridge with Asp414, interacts with Val422 carbonyl oxygen through H-bond. Structurally, this affects the arrangement of crystallographic dimerization interface which becomes more extended and presents two Glu412-Arg448 intermolecular salt bridges.

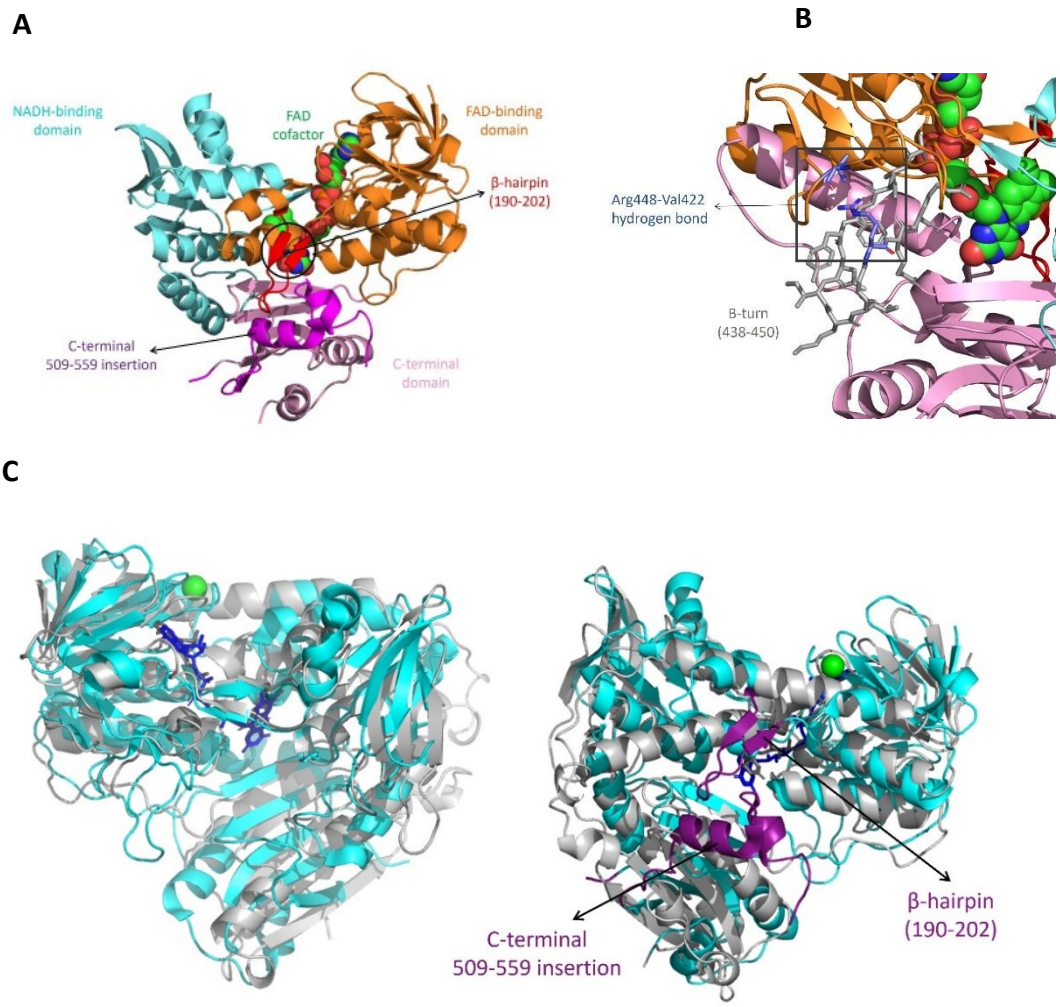

Fig. 1.3 Crystal structure of naturally folded murine AIFΔ1-77 (PDB: 3GD3). (A) FAD-binding domain, NADH-binding domain and C-terminal domain are depicted in orange, cyan and pink cartoons, respectively. FAD cofactor is in a green spheric representation. The β hairpin (190-202) and the C-terminal insertion (509-559) are represented, as unique features of AIF, in red and violet. (B) The characteristic β turn (438-450), found in naturally folded protein structure, is shown in grey licorice mode and the residues Arg448 and Val422, forming a hydrogen bond, in blue. (C) Structural comparison between AIFΔ1-77 and human glutathione reductase (PDB: 1BWC)(10), represented in cyan and grey respectively. The

peculiar structural features of AIF, β-hairpin and C-terminal portion between residue 509 and 559, are shown in purple.

In the same work, Sevrioukova *et al.* obtained the crystal structure of naturally folded NAD-bound AIFΔ1-101, with a resolution of 2.24 Å. This important study allowed a detailed analysis of redox properties of AIF (PDB: 3GD4).

1.2.4 AIF redox properties

GR family members are characterised by NADH- or NADPH-dependent reductase activity involving various electron acceptors. AIF is classified as a NAD-dependent enzyme with not yet identified endogenous substrates (12). However, its interaction with NAD(H) has the peculiarity to form a highly stable charge transfer complex (CTC) between $FADH^-$ and NAD^+. The CTC is an assembly between two molecules based on electrostatic forces where an electron donor transfers some of its electron density to an electron acceptor. The interaction causes electrostatic transitions which result in characteristic absorption spectrum bands of CTC. In this case, NADH represents the electron donor that can reduce the FAD cofactor in $FADH^-$, in turn becoming NAD^+. The formation of the charge transfer complex is also associated with conformational changes in protein structure leading to AIF dimerization. This effect suggests a possible role of AIF as a redox/NADH sensor inside mitochondria which, depending on the quaternary structure, assumes different functions as a part of a novel signal-transduction pathway.

As anticipated, important structural details regarding CTC formation derived from the crystal structure analysis of NAD-bound murine AIFΔ1-101 (11). AIF in complex

with NADH is a dimer, topologically similar to the crystallographic dimer of free AIF. However, in this case the dimer is closer and displays more hydrophobic and polar interactions at the dimerization interface, among which the electrostatic interaction between Arg448 and Glu412 seems to be particularly important to stabilise the dimer formation. Observing the crystal structure, it is possible to notice that NAD assumes an elongated conformation with its nicotinamide moiety positioned in a parallel manner to FAD isoalloxazine ring and stabilised by an additional stacking interaction with Phe309. The optimization of the π-π charge-transfer interaction between the nicotinamide and the flavin nucleotide part of FAD requires a shift of about 1.2 Å of the latter. Moreover, NAD in the active site is stabilised by the presence of two water molecules which interact with an extensive hydrogen bond network involving residues Lys176 and Glu313. Another important and peculiar feature of reduced AIF regards residue His453 in the active region. Upon NAD binding, His453 moves about 3.5 Å and forms H-bond with NAD(O7). This local conformational shift induces the movement of the 438-453 region which results in the stabilisation of the dimerization interface. However, the most relevant redox changes regard the C-terminal region of NAD-bound AIF. In particular, the displacement of Phe481 and Phe309 caused by the presence of NADH molecule induces the rearrangements of residues Tyr491, Trp578, Trp350, Tyr346, Phe507 and Tyr559 which align to form an aromatic tunnel from the active site toward the surface. More specifically, the new conformational disposition of these aromatic amino acids, located at a distance < 4 Å between each other, favours the delocalization of electrons which promotes CTC lifetime extension. Molecular studies on AIF reductase activity identified the role played by some residues in favouring the interaction between FAD and NADH cofactors in the active site. In particular, Lys177 and Glu314 amino acids have been found to favour the correct

holo-enzyme active site conformation; while residue Pro173 is important to set up the flavin environment and to regulate AIF affinity for NADH (13).

An additional and important effect at the level of C-terminal domain is the rearrangement of the 509-558 peptide (C-loop) (14). The NADH binding causes the unwinding of the α helix between residues 517 and 523 with a dramatic effect also on the β hairpin (190-202), which is exposed to the solvent. Recent mutagenesis experiments demonstrated that Trp195 of the β hairpin has an important role in maintaining proper compactness and stability of oxidised AIF and in triggering the C-loop released to the solvent in the reduced form of the protein. Moreover, it works as an electron leakage site suggesting that probably the hairpin displacement upon AIF reduction could mediate interactions and electrons transfer with partner proteins (15).

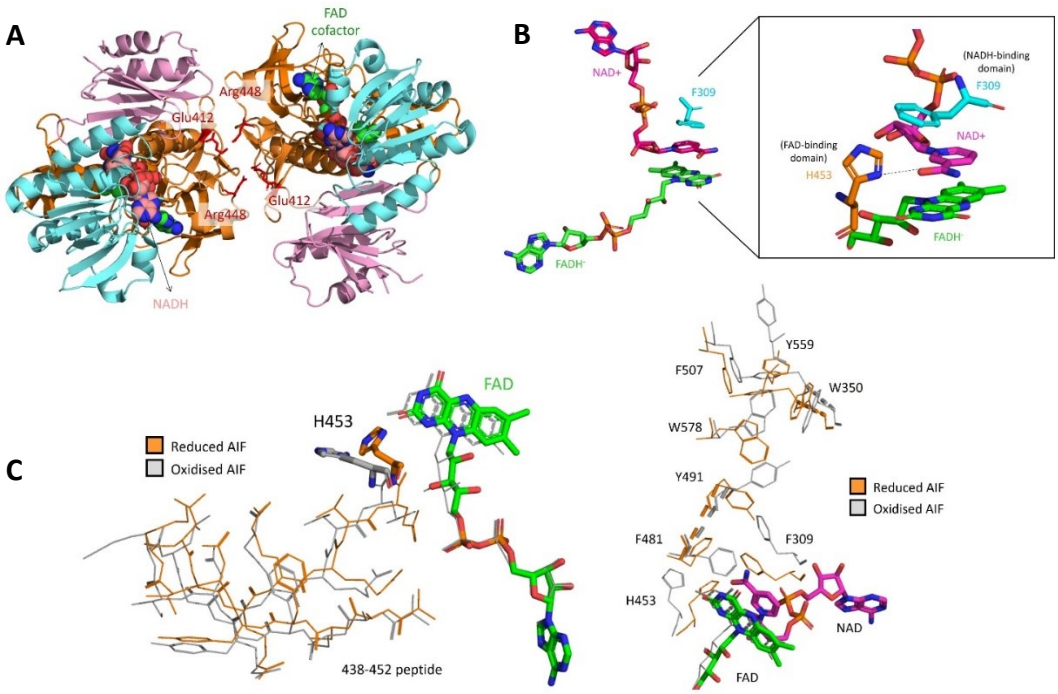

Fig. 1.4 Crystal structure of reduced murine AIF (PDB: 3GD4). (A) The dimeric/reduced form of AIF is represented with the same colour code of the oxidised one (Fig. 1.3). NADH molecules are represented as red spheres, and the residues Arg448 and Glu412, involved in the dimerization interface, are highlighted as sticks. (B) Structure of AIF active site when in CTC with NAD^+. NAD^+ nicotinamide ring (shown in magenta) is parallel stacked between the isoalloxazine of FAD (shown in green) and Phe309 (shown in light blue), establishing an H-bonding network with the surrounding residues. (C) His453, undergoes a large positional shift upon AIF reduction, causing the displacements of the 438-452 peptide which forms an aromatic tunnel from the active site towards the surface.

1.3 AIF role in apoptosis pathway

1.3.1 Release of mitochondrial AIF

AIF plays an important role in the intrinsic apoptotic pathway. Programmed cell death (PCD), depending on the stimulus, is executed upon the activation of either an extrinsic or an intrinsic pathway. The latter is triggered upon intracellular stress signals, induced by different stimuli such as DNA damage, oxidative stress or growth factor depletion. One of the main consequences of these stress signals is the mitochondrial outer membrane permeabilization (MOMP), as a result of the activation of some pro-apoptotic members of BCL-2 family. MOMP promotes the release in the cytoplasm of different pro-death proteins from the IMS (16). BCL-2 family members are classified into three functionally and structurally distinct subgroups: BH3-only proteins, pro-survival cell guardians such as BCL-2 itself, and pro-apoptotic effectors BAX and BAK. When BH3-only proteins receive apoptotic signals in response to different cytotoxic stresses, they carry out their apoptotic functions through two mechanisms: the neutralisation of pro-survival BCL-2 proteins

or the direct activation of the pro-apoptotic effectors BAX and BAK. Once activated, BAX and BAK form symmetric dimers constituting the core of the oligomers that perforate the mitochondrial outer membrane, even if the underlying molecular mechanism is still unsolved (17).

Among the factors released by mitochondria upon MOMP activation, AIF was the first protein shown to promote caspase-independent cell death. After MOMP, AIF is released in the cytoplasm, translocates to the nucleus where it causes chromatin condensation and DNA fragmentations, leading to cellular apoptosis. Even if the specific upstream components of the AIF death pathway are still under study, it is known that AIF is one of the intermembrane proteins that is released earlier. One of these components is poly (ADP-ribose) polymerase 1 (PARP-1), a nuclear enzyme involved in DNA repair mechanisms. After a DNA damage, indeed, PARP-1 synthesises polymers of ADP-ribose and transfers them to acceptor proteins, for example histones and topoisomerases, influencing their functions and promoting DNA repair. When the DNA damage is unrepairable, PARP-1 activates a caspase-independent pathway based on the mitochondrial release of AIF through the dissipation of the mitochondrial membrane potential and the alteration of Ca^{2+} homeostasis (18). The translocation of AIF in the cytoplasm requires the proteolytic cleavage of the N-terminal transmembrane portion of the protein in addition to MOMP. The truncation of AIFΔ1-54 is performed by Ca^{2+}-dependent μ-calpain or other proteases like cathepsins B, L, S.

1.3.2 Cytoplasmic interactions of apoptogenic AIF

Once in the cytoplasm, AIFΔ1-102 can interact with both pro-death and pro-survival proteins determining the cell fate. Interaction with different partners can be

influenced by AIF redox state: oxidised AIF possesses a higher tendency to induce apoptosis, while reduced dimers have a higher affinity for pro-survival proteins. One of the cytoplasmic pro-life partners of AIF is Hsp70, a conserved molecular chaperone crucial for cell viability. Hsp70 promotes protein folding and translocation across cellular membranes, degradation of misfolded proteins, regulation of complex composition and signalling pathways modulation. When Hsp70 interacts with AIF, especially in its reduced and dimeric form, postpones or prevents the initiation of proapoptotic events inside the nucleus (19). Another pro-survival partner of AIF in the cytoplasm is the X-linked Inhibitor of Apoptosis Protein (XIAP), a member of IAPs family known to bind and inhibit caspases. Even if the specific underlying mechanism is still unknown, the interaction between AIF and XIAP seems to both modulate the activity of XIAP and reduce the cellular oxidative stress favouring cell survival (20). The cytoplasmic pro-death partners of AIF are eIF3 (eukaryotic translation initiation factor 3), TULA (T-cell ubiquitin ligand) and CypA (cyclophilin A). eIF3 promotes the binding of the 40s subunit of ribosome to mRNA and therefore is essential for protein synthesis. The interaction of AIF inhibits the eIF3 machinery and the *de novo* synthesis of proteins in addition to apoptosis signalling amplification through caspase 7 activation and cleavage of eIF3g subunit (21). TULA, instead, is a cytoplasmic protein which prevents c-Cbl-mediated inhibition of protein tyrosine kinases and epidermal growth factor, promotes c-Cbl degradation and cellular transformation. The AIF-TULA complex seems to amplify the apoptotic cascade through the interaction with other cytoplasmic factors (22). Finally, the main pro-death partner of AIF is CypA. Cyclophilin A is the most abundant and ubiquitous member of cyclophilins and is involved in cardiovascular diseases, cancer and viral infection pathogenesis and cellular biochemistry. AIF interacts with CypA in the cytoplasm and together they translocate to the nucleus. This interaction

occurs predominantly when AIF is in its oxidised/monomeric form and favours the AIF binding to DNA and other nuclear components promoting chromatin lysis (23).

1.3.3 Nuclear effects of apoptogenic AIF

The transport of AIF inside the nucleus is mediated by the presence of two nuclear localization sequences (NLS), surface peptides recognised by nuclear transport receptors which generally contain positively charged amino acids. NLS1 and NLS2 correspond to portion 277-301 and 445-451, respectively, in the sequence of murine AIF. Also for the nuclear import, the redox state of the protein seems to be crucial: while in the oxidised form of AIF, NLS2 is fully exposed and easily recognisable by nuclear receptors, the dimerization of the protein upon reduction buries the peptide hindering the nuclear import.

Inside the nucleus, AIF directly binds DNA through electrostatic interactions of a continuous patch of basic residues with the negatively charged sugar-phosphate backbone of DNA. AIF causes peripheral chromatin condensation and large scale DNA degradation through the displacement of chromatin-associated proteins and/or the recruitment of proteases and nucleases which form degrading complexes known as degradosomes (8). AIF acts as a platform for the assembly of degradosome components as phosphorylated histone H2AX and nuclease CypA. In particular, the AIF-H2AX interaction promotes the CypA latent nuclease activity and the nuclear cotransport of AIF and CypA has been found to promote DNA degradation in hypoxia-ischemia damaged neurons (24). However, recent studies demonstrated that AIF acts as a nuclease itself promoting DNA fragmentation alone or in cooperation with CypA. Two sites on human AIF have been identified as nuclease

motifs: the TopIB-like motif (residues Y443, K446, R449, R450, R451, and H454) and the DEK motif (residues D489, E522, and K510 or K518), near H2AX binding site (25).

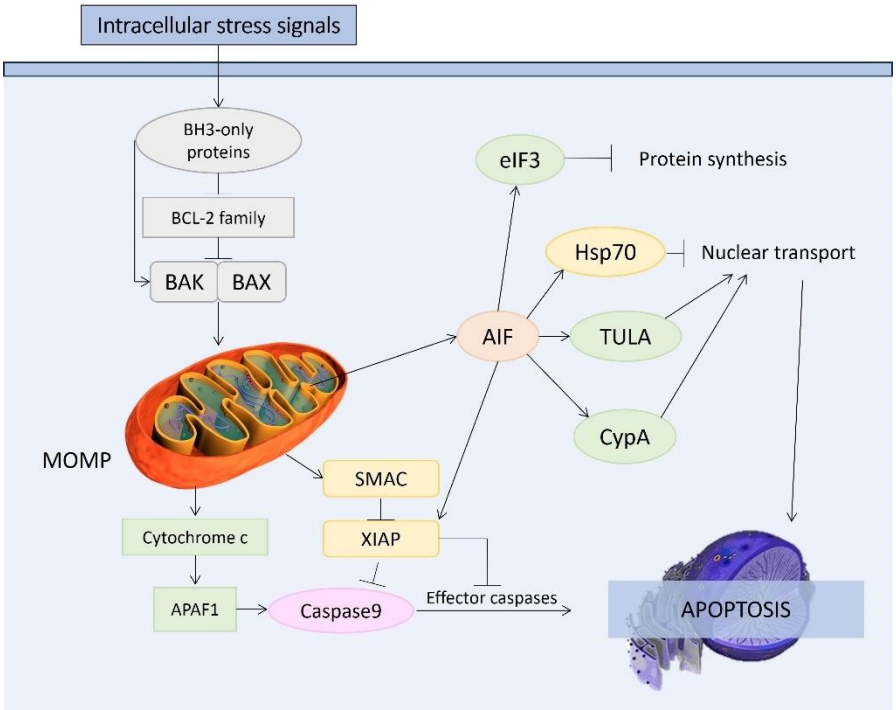

Fig. 1.5 AIF mitochondrial release process and interactions with cytosolic proteins. The scheme reports the BCL-2 family members involved in mitochondrial outer membrane permeabilization which causes the cytosolic release of apoptogenic AIF. Moreover, the principal pro-survival and pro-death interacting proteins of AIF are represented with their respective cellular functions.

1.4 Pro-survival functions of mitochondrial AIF

1.4.1 Oxidative phosphorylation in mitochondria

The mitochondrial oxidative phosphorylation process (OXPHOS) regulates the cell energy homeostasis, producing ATP from the electrochemical gradient of mitochondrial membrane. OXPHOS uses the electrons derived from NADH or $FADH_2$ and transfers them, through an electron transport chain (ETC), to the oxygen as the final electron acceptor which is reduced to water. ETC is formed by different complexes: NADH dehydrogenase (complex I), succinate dehydrogenase (complex II), ubiquinone, cytochrome bc1-complex (complex III), cytochrome c (Cyt c) and cytochrome c oxidase (complex IV). Coupled to electron transport in the ETC, complexes I, III and IV have also a proton pump activity which creates a proton motive force Δp_m across the inner membrane of mitochondria. Δp_m is composed by an electrical ($\Delta\Psi_m$) and a chemical part (ΔpH): Δp_m (mV) = $\Delta\Psi_m$ – 59 ΔpH. The ATP synthase (complex V) uses this Δp_m, associated to the backflow of protons from the mitochondrial intermembrane space to the matrix, to convert ADP and phosphate in ATP (26). This process of OXPHOS to generate ATP from an electrochemical gradient was firstly described by Peter Mitchell in 1961 and it has been found to provide 15 times more ATP than that produced in anaerobic glycolysis.

The regulation of OXPHOS complexes occurs at different levels depending on the organism. While in bacteria the respiratory chain complexes activity is regulated primarily by substrate availability and membrane potential, in higher eukaryotes there are additional regulatory mechanisms such as expression of tissue-specific isoforms, allosteric regulation and reversible phosphorylation. Many medical studies attribute to mitochondrial dysfunctions various pathologies among which diabetes, cancer, ischemia and neurodegenerative diseases. The malfunction of the

respiratory chain is often associated with human diseases due to lack of energy and/or excessive free radical production. Therefore, regulation of the cell energy homeostasis and consequently the biogenesis and the function of OXPHOS complexes is crucial for mitochondrial functionality. Flavoproteins have been found to play an important role in morphology regulation of mitochondria and energy metabolism.

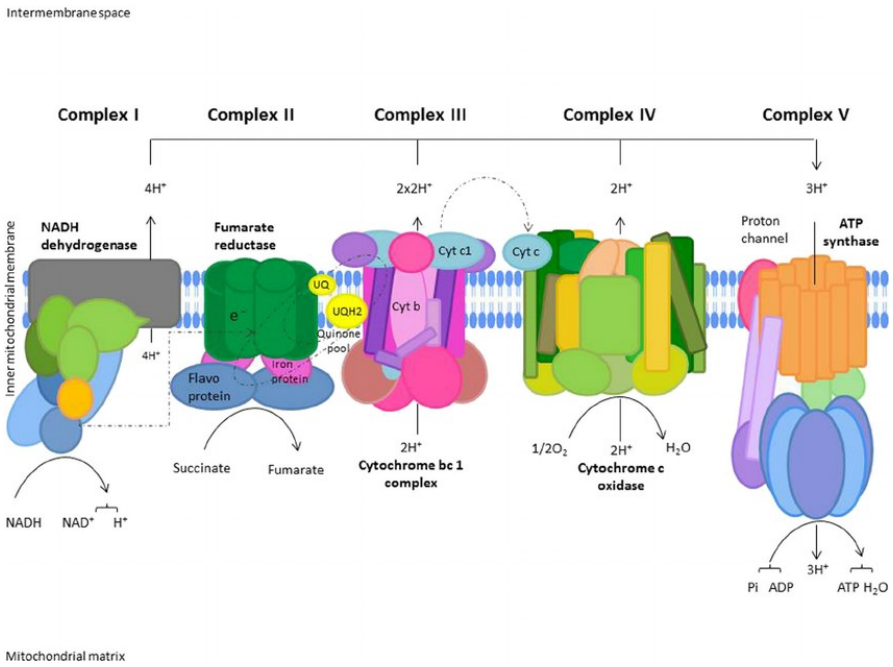

Fig. 1.6 Respiratory chain complexes involved in oxidative phosphorylation system (OXPHOS). Granata et al. (27)

1.4.2 Role of AIF in mitochondrial respiration and morphology

Over the past years, many studies attributed an essential pro-survival role to mitochondrial AIF in addition to its apoptogenic function. The phenotypes related to

AIF deficiency or mutations in cells, animal models or human patients revealed the role of the protein in important vital functions in mitochondria. The first studies regarded an *in vivo* model of AIF depletion in *Harlequin* (*Hq*) mice, generated by the insertion of a retrovirus in the first intron of the AIF gene. While the 80% decrease of AIF expression did not alter the mice phenotype at early age, adult mice showed hair lack, signs of neurodegeneration, ataxia, retinal degradation but were resistant to weight gain and lipid accumulation. Analysing the neurons and cardiomyocytes of *Hq* mice, it was also possible to correlate AIF low levels to an increased sensitivity to peroxides and ROS-related damages (28). These results suggested a possible role of AIF as an antioxidant with a role in OXPHOS process and as an assistant in free radical scavenging, but this possibility was later rejected by *in vitro* experiments on isolated mitochondria (29).

Tissue-specific studies of AIF depletion effects were conducted to clarify the mitochondrial role of the flavoprotein. The analyses on mice with AIF knockout in cardiac and skeletal-muscle tissues showed severe dilated cardiomyopathy and skeletal atrophy. The metabolic investigation revealed that these animals presented reduced electron transfer associated with complex I and decreased ROS production (30). Moreover, the deficiency of AIF only in cortical neurons resulted in a lower cortical development and neuronal survival due to mitochondrial respiration alterations (31). All these findings, together with the evidence that only full length AIF expression could restore defects in complex I and cell growth function, suggest a role of this flavoprotein in supporting the OXPHOS process. In particular, AIF was proposed to regulate energy homeostasis by promoting biogenesis and stabilisation of complexes I and III (32). More recent studies associate AIF deficiency with mitochondrial electron transport chain (ETC) destabilization, correlated to transmembrane potential loss (33).

Since neurons generally have a higher energy demand and are not able to use aerobic glycolysis as an alternative to OXPHOS, their functionality is strictly correlated with mitochondrial metabolism. AIF low levels, indeed, cause oxidative damage and consequently neurodegeneration (31). Moreover, several studies on mice embryos characterised by AIF knockout in different neuronal cell types demonstrated that AIF is also crucial in neurogenesis and its lack is responsible for cell cycle alterations in a neuron-specific manner (34).

The architecture of mitochondria is essential for its metabolism and respiratory activity, therefore any defects in mitochondrial morphology is associated with metabolic and energetic alterations. Studies on a murine model lacking AIF gene in cortical neurons, reported mitochondrial aberrations in neurons such as size reduction, fragmentation, dilated cristae and membrane hyperpolarization. Since all these defects are repaired restoring the normal levels of AIF, a possible role of AIF in regulation of organelle morphology and cristae generation is suggested (31). Moreover, it has been demonstrated that AIF is able to form complexes with optic atrophy 1 (OPA1), cooperatively regulating and stabilizing multi-subunit complexes of the respiratory chain. OPA1 is a member of GTPase family and is responsible for mitochondrial fusion and fission and, therefore, for organelle morphology.

1.4.3 Mia40/CHCHD4

Most mitochondrial proteins are encoded in the nucleus and then synthesised as precursors in the cytoplasm. Mitochondria are formed by two membranes (outer and inner membrane), the inter-membrane space and the matrix. The mitochondrial import of proteins occurs through three main pathways which share the translocase TOM complex on the outer membrane and then a specific machinery which localises

the proteins in the right organelle compartment. (i) Many proteins present in the matrix have a N-terminal portion with positive charges. After the translocation through the TOM complex, they pass to the matrix thanks to the presence of the inner membrane TIM23 complex, a membrane potential-dependent pre-sequence translocase. Once in the matrix, the pre-sequence is then removed through proteolytic cleavage. (ii) Other proteins, especially of the inner membrane, do not have any cleavable N-terminal portion, but contain localization signal sequences. After passing through the TOM channel, they reach the inner membrane and are inserted in it through a separate machinery: Tim proteins assist the transport of the precursors through the IMS and promote their interaction with protein insertion complex on the inner membrane. (iii) Finally, the precursors of outer membrane proteins, as porins, are firstly imported in the IMS trough TOM complex and then, thanks to Tim proteins, are guided to the sorting and assembly machinery (SAM complex) on outer membrane. SAM complex favours their anchoring to the membrane and their association in functional complexes. However, there are many small proteins in the IMS which are not imported with any of these translocation pathways: an example are Tim proteins. In 2004, it has been identified a *Saccharomyces cerevisiae* protein, named Mia40, which binds precursors of Tim proteins, favours their translocation through the outer membrane and facilitates their assembly in IMS complexes (35). Chacinska et al. demonstrated that even if the precursor of Mia40 is imported, thanks to a bipartite pre-sequence, through the TIM23 complex, it is not required for the three previously mentioned import pathways. They also found out that Tim proteins are not the unique Mia40 imported proteins. Mia40, indeed, has a pivotal role in the IMS-import machinery of many small proteins. Interestingly, a common feature between these mitochondrial proteins is the presence of cysteine residues, responsible for metal ions coordination and/or disulphide bonds formation, both required for their import and folding.

In 2005, the human Mia40, also named CHCHD4, was identified and characterised by Hofmann et al (36). They found out that CHCHD4 (16 KDa) has a particular cysteine motif at its C-terminal part (CXC-CX_9C-CX_9C) and that these residues (from 47 to 102) are highly conserved among species, with a sequence similarity of 75% to *S. cerevisiae* and 98% to *Mus musculus*. The rest of the protein has a lower homology level between species. Moreover, while the fungal Mia40 has been demonstrated to be anchored to the inner membrane of mitochondria, human CHCHD4 is a soluble protein (37). This aspect was also observed in other higher eukaryotes such as *Drosophila melanogaster*, suggesting that the N-terminal transmembrane sequence is lost during evolution. Further analysis on CHCHD4 transcripts and expression patterns in different human tissues revealed that the protein has a ubiquitous distribution, with a predominance in liver, kidney, lung, brain and spleen. Regarding CHCHD4 cellular function, Hofmann and colleagues performed silencing experiments, using specifically designed siRNA, in HeLa cells. They observed that lower CHCHD4 expression levels are associated with a significant depletion of different IMS components, with a stronger effect on DDPI and Tim13 proteins. These results confirmed what was observed for yeast Mia40. Moreover, since CHCHD4 RNAs silencing does not affect other mitochondrial proteins like Hsp70 or cytochrome c, also for the human homolog was proposed a preference for cysteine-containing interacting proteins.

CHCHD4 is characterised by the presence of three highly conserved cysteine-pairs organised in one -CPC- motif and two -CX_9C- motifs. It has been demonstrated that these cysteines are involved in intramolecular disulphide bonds. The presence of CHCHD4 at different oxidation states inside the cells, therefore, suggests its role in repeated cycles of binding and release of IMS imported proteins. In addition to being important for the import of various proteins into the mitochondrion, the cysteine

residues of CHCHD4 play a fundamental role in the biogenesis and function of the protein itself.

More detailed knowledge about CHCHD4 activity was achieved after the structural characterisation of the protein by Banci et al. in 2009 (PDB: 2K3J) (38). They confirmed the presence of three cysteine pairs forming disulphide bonds and noticed that -CPC-motif was more easily reduced, by DTT, with respect to the other two -CX_9C-. This information firstly suggested a possible role of -CPC- in its redox activity. From the ^{13}C NMR structure of CHCHD4 it is possible to distinguish a small helix in residues 56-59 and two longer helices in the segments 65-77 and 88-100, named α1, α2 and α3, respectively. The rest of the structure, in particular the N and C-terminal portions, is not folded. CHCHD4 structure can be divided in a "core", composed of α2 and α3 forming a α hairpin and kept together by the two -CX_9C- motifs, and a rigid "lid" positioned onto the core. The lid does not adopt any secondary structure except for the α1 and residues Pro54 and Cys55, preceding α1, which show a small helical propensity. These two residues form, with Cys53, the CPC motif and, when the two cysteines are reduced, the CPC region is more structurally flexible and therefore critical for protein catalytic activity. Moreover, the hydrophobic residues on the lid directly interact with aromatic amino acids of the α hairpin. These interactions cause the CPC motif to be solvent-exposed and positioned over a hydrophobic cleft, composed of residues Leu42, Leu43, Ile49, Trp51, Leu56, Met59, Ala60, Phe68, Phe72, Phe91, Met94 and Met98, and responsible for proteins binding. On the opposite side of the α hairpin interacting with CPC, instead, there is a highly charged region.

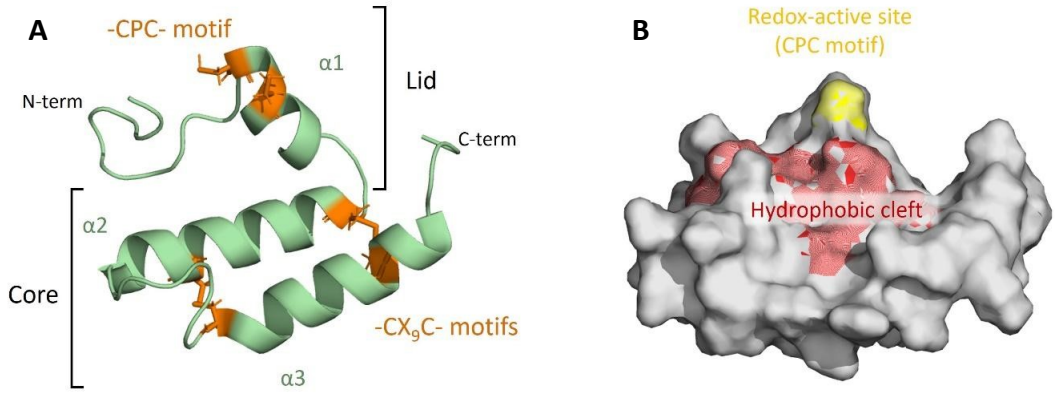

Fig. 1.7 Three-dimensional structure of human CHCHD4 solved by NMR. (A) Cartoon representation of CHCHD4. The N-terminal lid comprises the unstructured N-terminus and the α1, while the core portion of the protein is folded in α2 and α 3 with disordered C-terminus. Disulphide bonds in CPC and CX_9C motifs are shown in orange. (B) Surface representation of CHCHD4. The active site containing Cys55 of the CPC motif and the hydrophobic cleft in the protein core are represented in yellow and red, respectively.

The structural characterization of CHCHD4 supported its dual function in IMS as a substrate import receptor and protein folding oxidase. The hydrophobic cleft, present in the core portion of the protein, recognises and binds substrates through non-covalent interactions, making them available for oxidative folding. The N-terminal lid then is the functional site of the molecule with the oxidation-active CPC site which favours substrates folding through the introduction of disulphide bonds. It has been demonstrated that CHCHD4 shares with some of its mitochondrial substrates the presence of the α hairpin core with two -CX_9C- motifs, as COX17. For kinetic reasons, these proteins, that are imported in IMS in their fully reduced forms, cannot be oxidised only by oxygen but require the catalytic activity of CHCHD4.

Therefore, CHCHD4 initially introduces the first disulphide bond in the substrate and forces the other two cysteine of the second -CX_9C- site in a favourable position for the second disulphide bond, introduced finally by the oxygen. After its catalytic activity, the CPC motif is reduced and its reoxidation is ensured by the FAD-linked sulfhydryl oxidase Erv1 (ALR in humans).

1.4.4 AIF and CHCHD4 interaction

In 2015, Hangen et al. were able to correlate AIF and respiratory chain function, providing more detailed information about the physiological role of the protein inside mitochondria (39). Through immunoprecipitation experiments followed by mass-spectrometry analyses, they identified CHCHD4 as an interacting protein of AIF in IMS. The interaction between the two proteins turned out to be particularly strong even under unfavourable binding conditions, such as treatment with translation inhibitor cycloheximide (CHX), and pull-down assays proved a direct binding between them. Mutagenesis experiments on CHCHD4 cysteines do not alter its binding to AIF, indicating that the enzymatic active part is not implicated in the interaction. To clarify the binding region of CHCHD4, they performed several deletion mutagenesis experiments through which they found that the N-terminal portion of the protein, constituted by 27 residues, is sufficient for AIF interaction. However, deletions of different AIF domains produced proteins not able to bind CHCHD4. Moreover, different experiments showed that the complex formation between AIF and CHCHD4 is favoured when AIF is bound to NADH, in its reduced form.

Knockdown experiments of CHCHD4 resulted in lower expression levels of different respiratory chain subunits and defects especially in complexes I and IV, but no effects

on AIF. On the contrary, the reduction of AIF levels caused CHCHD4 depletion, without any alteration on its mRNA quantity. Moreover, the effects of AIF and CHCHD4 knockdown on respiratory chain complexes and CHCHD4 substrates were the same. All these results suggest that AIF regulates CHCHD4 expression levels, not vice versa, and that it acts upstream in the regulation of mitochondrial protein complexes biogenesis and function, including the subunits of the respiratory chain (40). Additional experiments also proved that CHCHD4 import in mitochondrial IMS is translation-dependent and is strictly related to AIF presence. Recent studies demonstrated that the negatively charged C-terminal region of CHCHD4 is crucial for the stabilization of the cytosolic protein precursor and that it slows down the import inside mitochondria. This stabilization of CHCHD4 in the cytosol might guarantee a persistent pool of the protein that is available for the import by AIF, accordingly to the IMS levels of NADH (41). Far-UV circular dichroism spectroscopy experiments demonstrates that the interaction between CHCHD4 and AIF causes important conformational changes in AIF-binding portion of CHCHD4 which affect the ability of the protein to interact with substrates (39).

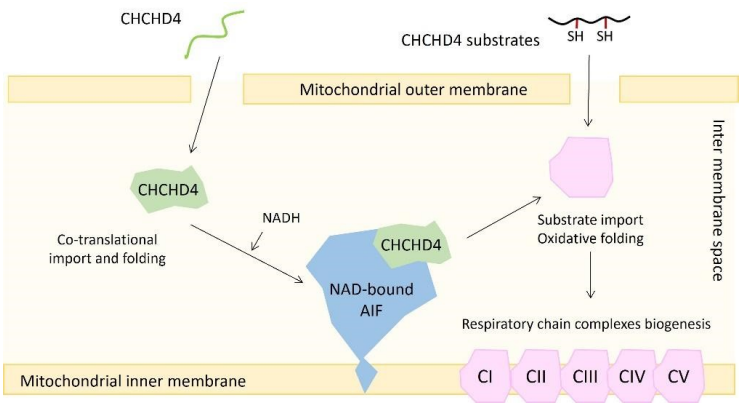

Fig. 1.8 Simplified representation of AIF-CHCHD4 interaction. After CHCHD4 precursor import in the IMS, the protein folds and interacts with AIF, especially in its reduced form.

AIF then supports the activity of CHCHD4 in promoting the oxidative folding of different substrates, including the proteins forming respiratory chain complexes (39).

1.5 AIF and CHCHD4-related diseases

1.5.1 AIF mutations

As already mentioned, mitochondrial functionality and, especially, OXPHOS processes are essential for neuronal metabolism, as unique sources for their high energy demand. Therefore, OXPHOS defects are always associated with neurodegeneration. AIF plays an important role in maintaining OXPHOS functionality and its deficiency has been shown to cause mitochondrial impairments and neuron loss. To date, more than twenties allelic variants of AIF have been characterised and correlated with mitochondriopathies, with neurodegeneration as a common feature (42,43). R201 deletion (44), G308E (45), G262S (46), G338E (47), T141I (48), Q479R (49) and T492H (50) substitutions have been found to provoke mitochondrial encephalopathies. V243L (51), F210S (52), F210L (53), M171L (54) and E493V (55) replacements cause peripheral symptoms like muscular atrophy, neuropathy and deafness with either early childhood or late onset, depending on the mutations. E493V substitution, in particular, is associated with a specific disease known as Cowchock syndrome. Q235H, D237V, A237V (56) and D237G (57) replacements, instead, cause skeletal deformities and hypomyelination, as additional features to progressive neurodegeneration. Finally, more than ten mutations at the level of AIF gene have been recently identified and correlated to familial or sporadic auditory neuropathies (48,58).

Since the AIF gene (AIFM1) is located on the X-chromosome, the inheritance of AIF-related diseases especially regards male infants. However, the molecular mechanisms at the basis of symptoms related to AIF depletions are not easily understandable due to the dual role of flavoprotein inside cells. Some efforts have been made in the last years to biochemically characterise AIF mutants. V243L, G262S and G338E replacements induce AIF levels reduction, probably altering protein folding and/or stability. Flavoprotein deficiency is consequently associated with impairments of respiratory chain complexes I and IV functionality. G262 residue is localised between FAD and NADH-binding domain, near the pyrophosphate group of FAD cofactor. In 2016, Sevrioukova et al. determined the crystal structure of G262S mutant and compared it to the wild type one (59). A ~1.0 Å shift was observed at the level of the isoalloxazine ring of FAD. To further investigate structural modifications in the AIF active site induced by the mutation, they also superimposed the G262S structure with the one containing V243L replacement, obtained with the same space group, since no alterations in the active site are expected for this mutant. They noticed a ~0.2 Å displacement of mononucleotide portion of FAD in G262S which consequently causes the rearrangement of Arg45, Glu53 and Leu400. These conformational changes reduce the flexibility of NADH binding site, promoting a faster oxidation of CTC and an enhanced AIF redox activity. G338E replacement, instead, was firstly characterised by Diodato and collaborators in 2015. The mutation is localised near the NADH binding site and therefore influences the CTC formation. AIF reduction causes the displacement of residues 510-560, responsible for protein localization, lifetime, post-translational modifications and interactions with other proteins or DNA. In reduced AIF this peptide is positioned near residue 338, therefore a modification at this site may also have functional consequences.

E493V substitution and R201 deletion increase the reduction rate of AIF by NADH and CTC reoxidation by oxygen. More in detail, for E493V mutation, neurodegeneration is due to an increase in AIF apoptogenic function; while with R201del, AIF seems to be more unstable and prone to FAD cofactor release. The R201 residue, indeed, is positioned at the level of the β hairpin responsible for protein conformational stability. The deletion does not alter AIF structure but reduces protein stability and makes it more prone to proteolytic cleavage. Consequently, the CTC formation is discouraged as well as FAD binding. A similar effect to that of R201 deletion is caused by G308E variant: this residue, highly conserved in vertebrate AIFs, occupies the second position in the canonical Rossmann fold GXGXXG, in the protein tunnel of NADH-binding domain. The biochemical analyses on AIF F210L mutant, instead, revealed that this variant is associated with a loss of respiratory chain protein subunits of complexes I and III.

D237G mutation was described for the first time by Mierzewska et al. in 2016, as the main cause of SEMD (sponsyloepimetaphyseal dysplasia) associated with mental retardation. The mutated residue is localised in the FAD-binding domain and, in particular, in the portion of β sheet exposed to solvent. Even if there is still no evidence about the structural consequences of replacement, the substitution of aspartic acid with a smaller residue probably causes the displacement of neighbour amino acids with the following alteration of FAD binding and AIF redox properties.

1.5.2 CHCHD4 expression levels alterations

CHCHD4-related diseases are principally due to the alterations of protein expression levels. CHCHD4 downregulation has been observed in patients suffering from Friedreich's ataxia, caused by deficiency of frataxin inside mitochondria normally

imported by CHCHD4 (60). On the other hand, CHCHD4 overexpression was reported in different cancer types as cause of tumour progression and reduced patient life expectations. In mammalian cells, it has been identified as responsible for p53 mitochondrial translocation under oxidative stress. Here, p53 protects mitochondrial DNA directly or by transmitting the signal to other proteins which perform the same function, although the underlying molecular mechanism is still unclear (61). Moreover, CHCHD4 promotes HIF1-α stability, an essential factor for hypoxia control. Hypoxia occurs when there is an oxygen reduction in some tissue areas and is strictly correlated with cancer progression and resistance to antitumoral drugs (62). Overexpression of CHCHD4 is often associated to the onset of hypoxia and, therefore, to decreased patient survival. Despite detailed knowledge about the molecular mechanisms which correlate CHCHD4 overexpression and tumour progression are still missing, recent studies demonstrated that CHCHD4 guarantees growth advantage to tumoral cells by promoting the functionality of respiratory chain complexes. Moreover, CHCHD4 overexpression causes the downregulation of genes important for the transition of epithelial cells to mesenchymal phenotype, a typical feature of metastasing cancers (63).

2. Aim of the project

The present PhD project was focused on the study of the FAD-dependent mitochondrial flavoprotein Apoptosis Inducing Factor (AIF) and its recently discovered interaction with the mitochondrial protein CHCHD4. After pro-apoptotic stimuli, AIF is cleaved by proteases such as μ-calpain and translocates into the nucleus in a soluble pro-apoptotic form. Inside the nucleus, AIF is able to recruit a series of nuclear proteins, bind DNA and promote DNA fragmentation, chromatin condensation and subsequent cell crushing. As many apoptotic factors, AIF is also known to have a pivotal pro-survival role. Although the underlying molecular mechanisms are not fully understood, recent studies indicate that AIF is able to regulate mitochondrial morphology and oxidative phosphorylation (OXPHOS). This important role is played thanks to its interaction with CHCHD4 (coiled-coil-helix-coiled-coil-helix domain containing 4 protein), involved in the import and assembly of respiratory complexes subunits. This finding provided for the first time a clear connection between AIF and OXPHOS and shed new light on the AIF vital role. Furthermore, different distinct point mutations of the AIFM1 gene, localised on the X chromosome in humans and mice, were found to cause severe mitochondriopathies, with neurodegeneration as a common feature. Some of these pathogenic variants of the flavoprotein were biochemically characterised and well defined alterations in AIF molecular properties were associated with the neurodegenerative disorders they caused. However, some mutants still lack a thorough biophysical characterization. Since their pathological mechanisms could be related to alterations in AIF-CHCHD4 complex activity, the understanding of AIF physiological function in mitochondria represents an important step forward in the identification of these mutation's effects. Moreover, the elucidation of AIF molecular

properties of its physiopathology could help the development of effective therapies for the various and growing diseases associated with this flavoprotein.

Therefore, the main aim of the present PhD project was the structural and functional characterization of the complex formed by AIF and CHCHD4. In particular, we were interested in (i) studying the effects of CHCHD4 binding on the catalytic activity of AIF and its interaction with NAD^+/H, (ii) defining the binding properties of the complex (binding affinity, molecular interaction mechanisms, thermodynamic parameters), and (iii) identifying the putative binding site of the flavoprotein for CHCHD4. For the study of CHCHD4 binding effect on AIF active site reactivity we performed spectrophotometric assays, employing both the full length form of murine CHCHD4, whose production and purification protocols were optimised, and its 27-mer N-terminal peptide, sufficient for AIF binding. The binding properties of the complex were then explored through different biophysical techniques: analytic size exclusion chromatography for the study of complex stability and stoichiometry, ThermoFAD analysis for the investigation of CHCHD4 binding effects on AIF thermal stability, Microscale Thermophoresis (MST) experiments for the determination of binding affinities and Isothermal Titration Calorimetry (ITC) assays for thermodynamic parameters estimation. Once assessed the functional effects of CHCHD4 binding on AIF and the biochemical and biophysical features of their interaction, we focused more on the complex structure determination. Through the integration of different structural methodologies, such as AlphaFold model prediction, mass-spectrometry analysis on cross-linked complex and X-ray crystallography studies, we were able to acquire important structural information about CHCHD4 and AIF interaction. Finally, we validated the AIF binding site for CHCHD4 by mutating important AIF residues involved in the binding and testing the mutant through various techniques.

3. Results and discussion

3.1 Optimization of the CHCHD4 production procedure

3.1.1 Expression and purification of murine CHCHD4

The synthesis and purification protocols of recombinant CHCHD4 were initially designed including bacterial culture induction of about 2 h and protein isolation by an affinity capturing step followed by a gel filtration polishing step. If required, the removal of the His-tag was performed on the purified fusion protein. Since the yield in the final product was quite low, the whole procedure was optimised, incrementing both protein expression level and homogeneity of the purified protein. The pET-21a(+) vector, containing the mouse CHCHD4 coding sequence (pET-CHCHD4), was transformed into *E. coli* Shuffle® T7 strain. The expression yield in 2×YT medium was improved by lowering the growth temperature to 20 °C, after the induction with 0.2 mM IPTG, and extending the induction duration to about 16 h. From 2.5 L of culture, 4 g of cells were obtained. The induced cells were then harvested, lysed and the supernatant was loaded on a 5 ml HisTrap HP cartridge (GE Healthcare) equilibrated in solvent A (50 mM Tris-HCl, pH 8.0, 200 mL NaCl, 10 mM Imidazole, 10% glycerol). After a preliminary step at 2% of solvent B (50 mM Tris-HCl, pH 8.0, 200 mL NaCl, 500 mM Imidazole, 10% glycerol) to eliminate non-specifically bound proteins, a gradient from 2% to 100% of B was applied (Fig. 3.1 (A)). Protein was collected at about 35-45% B, after a peak of contaminants. Imidazole excess was removed from the fraction using a 53 ml HiPrep ™ 26/10 Desalting (GE healthcare) column (Fig. 3.1 (B)).

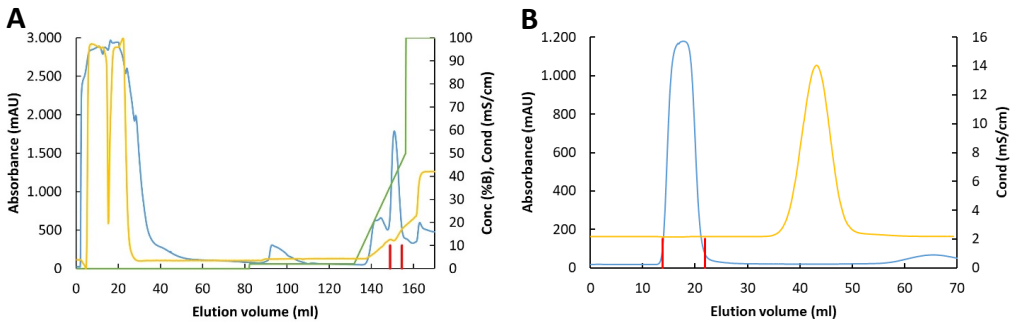

Fig. 3.1 Chromatograms of the first purification step of CHCHD4. (A) Ni-affinity chromatography profile of CHCHD4, whose peak is indicated between two red lines. (B) Desalting step chromatogram showing the buffer exchange.

Improvement of the homogeneity of the isolated protein was then obtained by replacing the gel filtration chromatography used in the previous protocol with anion exchange as the second purification step. To avoid non-physiological oligomerization driven by intermolecular disulphide bonds formation between N-terminal free cysteine residues, 5 mM DTT was added to protein fraction. CHCHD4 was then loaded on a 20 ml HiLoad ™ 16/10 Q Sepharose HP column, equilibrated in solvent A (50 mM Tris-HCl, pH 8.0, 10% glycerol) and eluted at about 40-50% solvent B (50 mM Tris-HCl, pH 8.0, 1 M NaCl, 10% glycerol), using a gradient from 0% to 100% B in 5 column volumes. A final desalting step was performed, using two HiTrap ™ desalting cartridges connected in series and equilibrated in the storage buffer (50 mM Tris-HCl, pH 7.4, 10% glycerol). Isolated protein was then brought to anaerobic conditions to avoid the oxidation of N-terminal free cysteine residues by oxygen. The optimization of production protocol allowed to increase the final protein yield to 2.3 milligrams per gram (fresh weight) of *E. coli* cells.

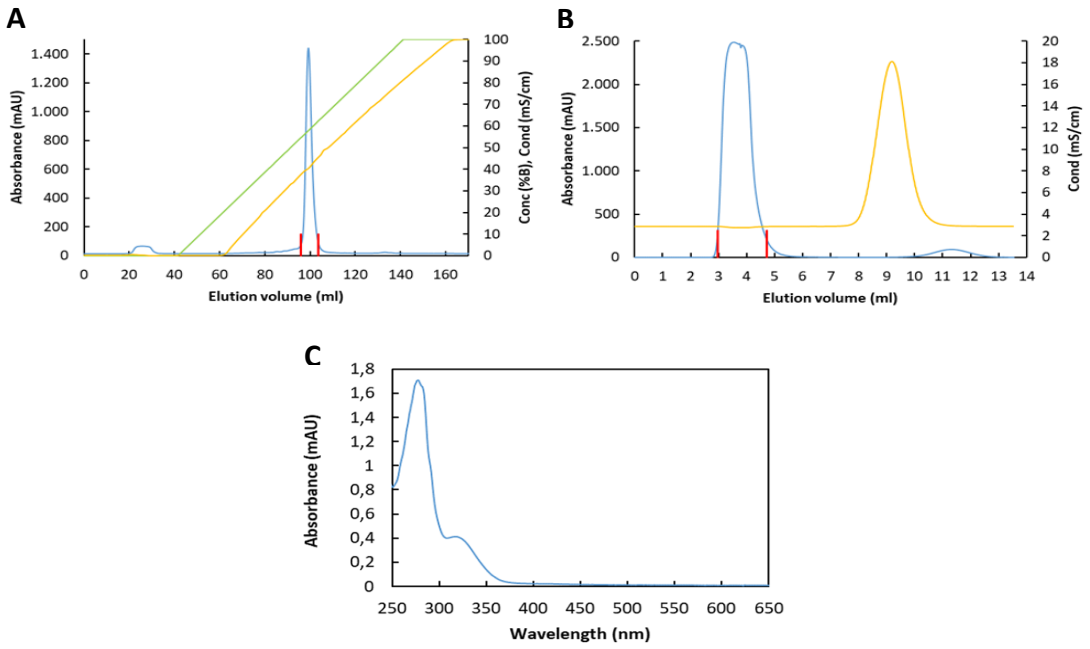

Fig. 3.2 Chromatograms of the second purification step of CHCHD4 and absorption spectrum of the isolated protein. (A) Anion exchange chromatography profile. CHCHD4 corresponding peak is highlighted between the two red lines. (B) Final desalting step, through which the salt excess is removed before protein storage. (C) Absorption spectrum of purified CHCHD4 with an absorbance maximum at 280 nm. Protein concentration is calculated using an extinction coefficient at 280 nm of 13.325 $mM^{-1}cm^{-1}$.

3.1.2 Protocol optimization for CHCHD4 His-tag removal

Microscale Thermophoresis experiments are based on the detection of temperature-dependent changes in fluorescence of a target as a function of the concentration of a non-fluorescence ligand (64). The fluorescent target in our studies is AIF, which is labelled on the His-tag by the red fluorescent dye NT-647, while the ligand is CHCHD4 or its N-terminal peptide. Synthetic peptide of the first

N-terminal 27 residues of CHCHD4 was synthesised in collaboration with the Department of Biochemistry of Milan with the following sequence: MSYCRQEGKDRIIFVTKEDHETPSSAE. According to manufacturer directions, the ligand should not contain any His-tag to prevent possible interference in subsequent analyses due to sequestration of the label. Therefore, we optimised the protocol for the removal of C-terminal His-tag from CHCHD4, exploiting the presence of a thrombin cleavage site. To set up the optimal conditions for cleavage protocol, we tested different protein/thrombin ranges and incubation times. In particular, we prepared three mixtures containing 0.01, 0.004 or 0.001 thrombin unit per µg of CHCHD4, and we stopped each cleavage reaction after 30 min, 1 and 2 hours of incubation at 25 °C. The samples were analysed by SDS-PAGE electrophoresis and, as shown in Fig. 3.3, a band slightly under that of His-tagged CHCHD4 was obtained for all the conditions tested, indicating successful tag removal.

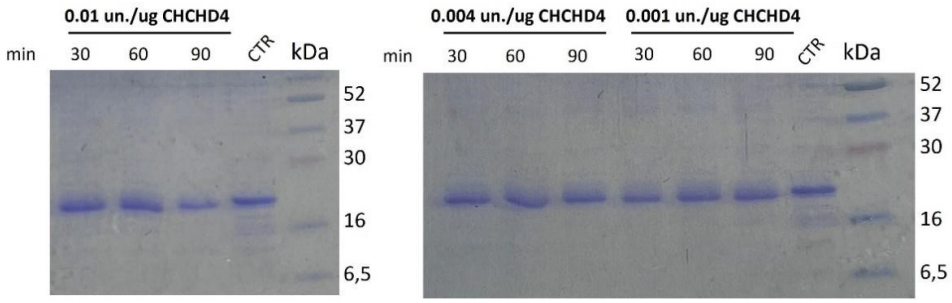

Fig. 3.3 SDS-PAGE analysis of thrombin cleavage optimization of CHCHD4 His-tag. His-tagged CHCHD4 was incubated for 30 minutes, 1 hour and 2 hours at 25°C with 0.01, 0.004 or 0,001 units of thrombin per µg of protein. CTR lane corresponds to CHCHD4 incubated in the absence of thrombin.

For the large-scale production of cleaved CHCHD4, we introduce the thrombin cleavage step after Ni-affinity chromatography, adding 0.005 unit of protease per µg of CHCHD4 and incubating the mixture for 1 h at 25 °C. To remove undigested residual protein, the mixture passed on a His-Trap HP column (Cytiva) before the anion exchange chromatography step. The purification of the untagged protein continued following the protocol already described for the uncleaved forms of CHCHD4. Through this optimised protocol, a yield of 1.8 mg of untagged CHCHD4 per gram of *E. coli* cells was obtained.

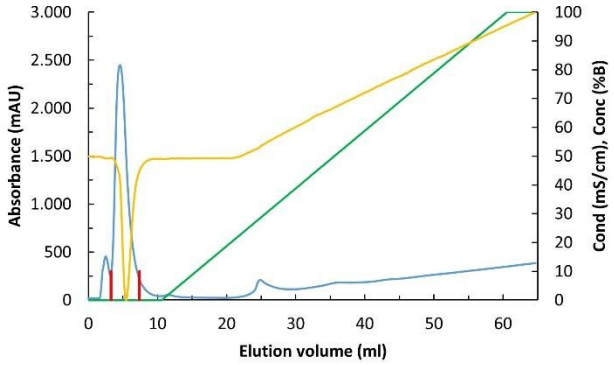

Fig. 3.4 Profile of Ni-affinity chromatography to remove possible residual His-tagged CHCHD4. The peak corresponding to cleaved CHCHD4 elutes in the flow-through fraction and is highlighted between the two red lines.

3.2 Analysis of the allosteric perturbation of the FAD microenvironment of AIF induced by CHCHD4 binding

3.2.1 Determination of the difference absorption spectrum of the AIF-CHCHD4/peptide complex

Alterations of FAD microenvironment in the AIF active site are expected to result in a perturbation of its absorption spectrum. Binding events, therefore, can be detected by monitoring the FAD spectral features. The visible spectrum of oxidised AIF was determined both in absence and in presence of CHCHD4, after an incubation of 30 min. Spectrophotometric measurements were performed also in the presence of 200 mM NaCl, to test the effect of ionic strength on complex formation. The results show that CHCHD4 induces an alteration in the FAD absorption spectrum as a consequence of binding, resulting in a characteristic difference spectrum with negative peaks at 455 and 487 nm. Moreover, low ionic strength increases the intensity of FAD spectral perturbation without any modifications in its shape.

To test the hypothesis that the N-terminal peptide of CHCHD4 induces the same AIF spectral variations of the full length protein, the visible spectrum of AIF was recorded before and after the addition of an excess of the peptide. As shown in the difference spectrum, the N-terminal peptide has the same qualitative effect on FAD microenvironment as the entire protein, however less intense. Therefore, although the peptide of CHCHD4 is sufficient for the interaction with AIF, the rest of the protein is needed to efficiently influence AIF active site.

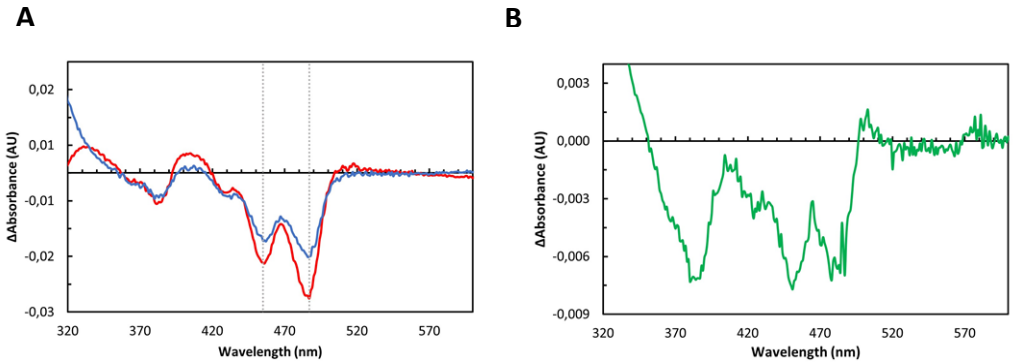

Fig. 3.5 Effect of the binding of CHCHD4 or its N-terminal peptide to AIF on the absorbance spectrum in the visible region. (A) Difference spectra calculated by subtracting from the spectrum recorded in the presence of CHCHD4 that recorded in its absence, at low (red) or high (blue) ionic strength. Two grey lines indicate the minima in the difference spectra at 455 and 487 nm. (B) Difference spectrum of AIF in presence of CHCHD4 peptide.

3.2.2 Preliminary study of the kinetics of CHCHD4 binding to AIF

The appearance of the difference spectrum due to complex formation between AIF and CHCHD4 was monitored over time for 60 min at 25 °C to have a qualitative indication of the kinetics of the process. The spectral change resulting from CHCHD4 binding is not complete after 1 hour, suggesting a low binding rate or a slow conformational rearrangement after a fast formation of an initial complex.

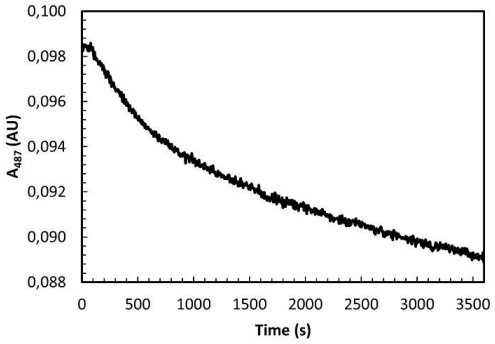

Fig. 3.6 Time course of the perturbation of the AIF spectrum upon CHCHD4 binding. The trace represents the progress of the A487 decrease after CHCHD4 addition.

3.3 Kinetic analysis of the catalytic activity of AIF under steady-state conditions

3.3.1 NADH-DCIP activity assay

Once ascertained that CHCHD4 and its N-terminal peptide are able to interact with oxidised AIF modulating its active site, the focus was to study the effect of this binding on the catalytic activity of AIF. In particular, we decided to test the possible effects of peptide binding, since preliminary experiments showed that its binding kinetics is significantly faster than that of the full-length protein. It is well known that AIF catalyses the reduction of the artificial dye 2,6-dichlorophenolindophenol (DCIP) by NADH and that the process can be easily monitored following the decrease of A_{600} resulting from DCIP reduction. The DCIP-NADH reduction occurs through two half reactions: the hydride transfer (H^-) from NADH to the AIF FAD cofactor and the subsequent reoxidation of FAD by DCIP. Since the rate of the second step is much faster, the assay measures the rate of reduction of AIF by NADH. To see the possible effect of CHCHD4 peptide on the catalytic activity of AIF, the DCIP-NADH reaction

was studied under steady-state conditions by varying the NADH concentration at a fixed concentration of DCIP, in absence and in presence of 0.7 µM peptide. By interpolating the kinetic data, a K_m of 0.7 ± 0.2 mM and a k_{cat} of 0.6 ± 0.1 s^{-1} were measured in the case of free AIF. The presence of the peptide significantly decreases the K_m to 30 ± 3 µM while increases the k_{cat} to 1.2 ± 0.04 s^{-1}. These results can be interpreted as an increased affinity of AIF for NADH induced by the interaction with the CHCHD4 N-terminal peptide.

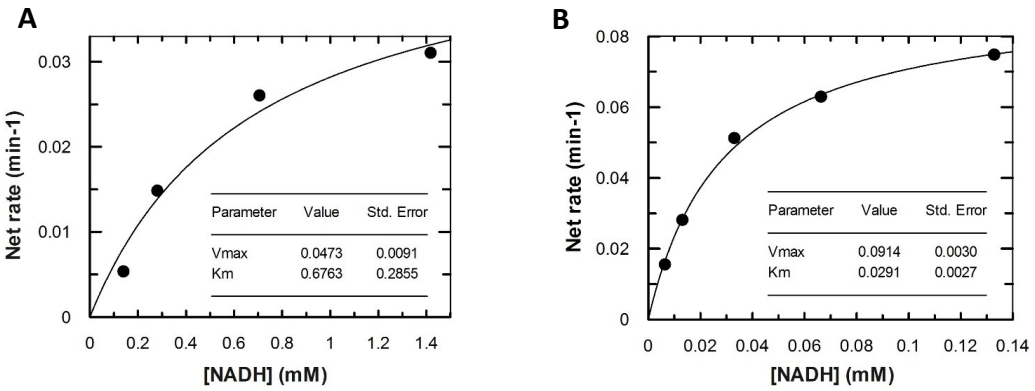

Fig. 3.7 Effect of the presence of CHCHD4 N-terminal peptide on the NADH-DCIP reductase catalytic activity of AIF. The rate of the reaction catalysed by AIF at different NADH concentrations measured in the absence (A) and in the presence of 0.7 µM CHCHD4 N-terminal peptide (B) are shown, one replicate per experiment.

3.3.2 Titration of the NADH-DCIP activity of AIF in presence of CHCHD4 N-terminal peptide

To quantify the effect of CHCHD4 peptide on the catalytic activity of AIF and to have an estimation of peptide dissociation constant, the rate of NADH-DCIP reduction process was monitored at a fixed concentration of NADH (100 µM) and varying the quantity of the peptide (0.06-1.98 µM). Results are reported in Fig. 3.8 and the interpolation of the data gave an estimation for the apparent K_d of AIF and peptide complex of about 0.4 ± 0.1 µM.

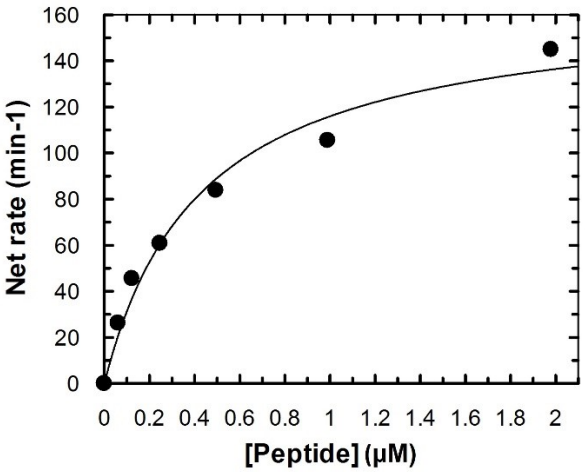

Fig. 3.8 Estimation of CHCHD4 N-terminal peptide binding affinity for AIF. Titration of AIF reductase activity with CHCHD4 peptide allowed to calculate a K_d of about 0.4 ± 0.1 µM.

3.4 Study of the effect of CHCHD4 binding on AIF interaction with NAD^+

3.4.1 Determination of the difference absorption spectrum of the AIF-NAD^+ complex in presence of CHCHD4

Once observed that peptide binding increases the affinity of the AIF active site for NADH, modulating its reactivity, we tested the hypothesis that the peptide interaction may also promote the binding of NAD^+. It is indeed known that the ability of oxidised AIF to bind NAD^+ is negligible, and that FAD cofactor reduction dramatically increases the affinity for NAD^+. The change in the absorption spectra of AIF induced by the presence of NAD^+ was investigated in the absence and in the presence of the peptide. While in the absence of the peptide no perturbations are detected, in its presence a significant red-shift in FAD absorbance is observed. We concluded that the peptide induces conformational changes in AIF active site, which promotes the binding of NAD^+ even to the oxidised form of AIF. The same analysis was performed also with full length CHCHD4 protein obtaining qualitatively equivalent results.

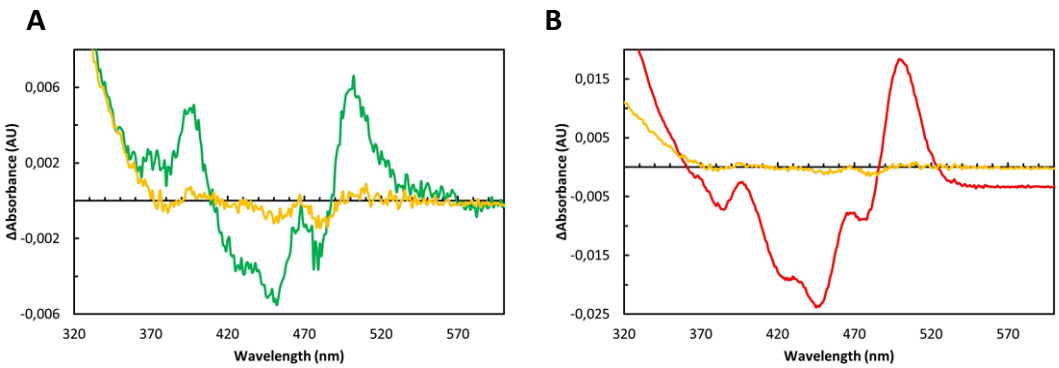

Fig. 3.9 Allosteric effect of CHCHD4 or peptide binding on the affinity of AIF for NAD^+. (A) Effect of the presence of NAD^+ on the absorbance spectrum of AIF in the absence (orange difference spectrum) and in the presence (green difference spectrum) of CHCHD4 peptide

at 25 °C. (B) Difference absorption spectra of AIF in presence of NAD^+ alone (orange) or of both NAD^+ and CHCHD4 (red).

3.4.2 Thermodynamic characterization of NAD^+ binding to AIF in presence of CHCHD4 peptide

To estimate the thermodynamic parameters of the binding process between AIF and NAD^+, favoured by the presence of the peptide, the temperature-dependence of the complexation was studied. The experiments were carried out in presence of AIF, NAD^+ and CHCHD4 peptide within a temperature range from 30 °C to 4 °C and recording spectra at intervals of about 2 °C. From the spectral series it is possible to observe a very strong thermal effect induced by the temperature change. In particular, as the temperature is decreased, the spectrum in the visible region of AIF becomes progressively less intense and red shifted. These findings suggest an increase in NAD^+-bound fraction of AIF as the temperature is decreased, reaching saturation at about 10 °C. The analysis of the difference spectra confirmed the results, showing negative peaks at 450, 480, and 502 nm.

To prove that the spectral transitions are directly due to the temperature and not to an indirect effect of the temperature on the pH of solution (due to the high thermal coefficient of Tris buffers), spectral variations at different pH were evaluated. The visible spectrum of AIF-NAD^+ complex in presence of CHCHD4 peptide was recorded at 25 °C before and after the addition of an amount of NaOH that mimics the pH change expected for a Tris-HCl buffer system shifting from 25 °C to 4 °C. No significant spectral changes were recorded proving that the temperature has a direct effect on the affinity of AIF for NAD^+, allosterically triggered by the CHCHD4 peptide (not shown).

Next, we considered the possible effects of the temperature on the spectrum of AIF in the absence of interactors and in presence of NAD^+ or CHCHD4 peptide alone (Fig. 3.10 (C)). No significant variations in FAD absorption spectrum were observed in all control experiments.

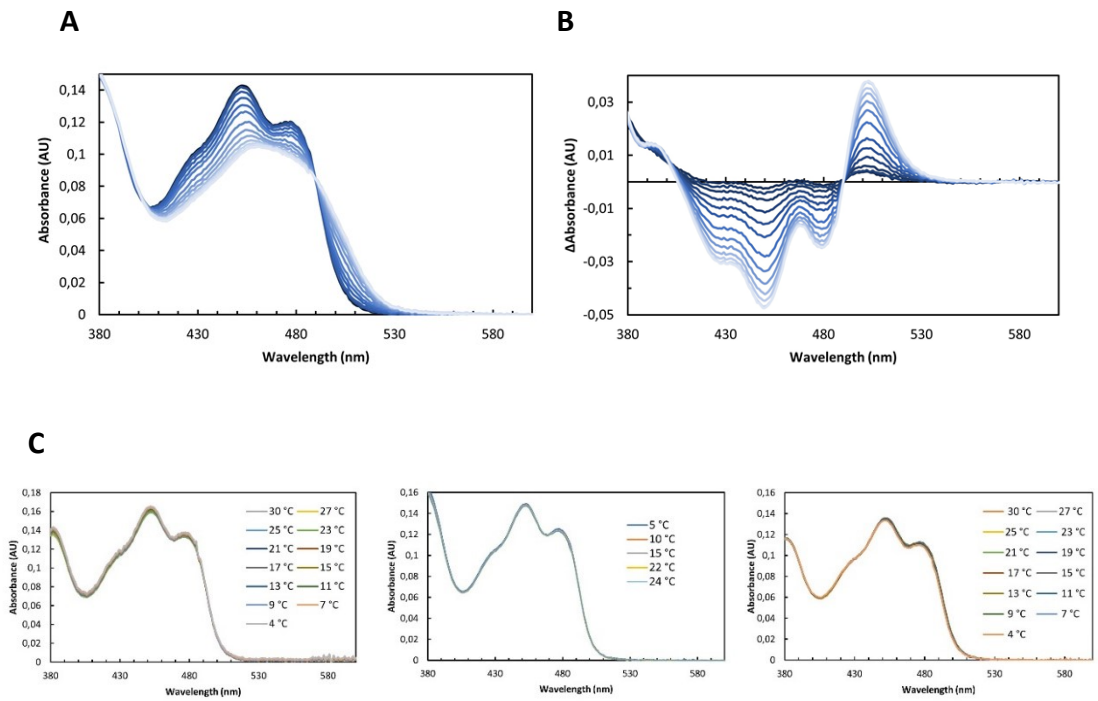

Fig. 3.10 Effect of the temperature on NAD^+ complexation upon N-terminal peptide binding to AIF. (A) Spectra and (B) difference spectra (calculated by subtracting the spectra of AIF and NAD^+ at the same concentrations) of the mixture containing 12.1 µM AIF, 139 µM CHCHD4 peptide and 6.24 mM NAD^+ at a temperature going from 30 °C (dark blue) to 4 °C (light blue). (C) Control experiments: FAD absorption spectra of AIF alone (left), AIF with NAD^+ (centre) and AIF with the peptide (right) at different temperatures.

3.5 Study of the effect of CHCHD4 binding on the reactivity of AIF towards thiol groups

The possible role of AIF in supporting the catalytic activity of CHCHD4 is currently not well described. To shed light on the contribution of AIF on disulphide oxidoreductase activity of CHCHD4, we evaluated the reactivity of AIF towards model sulfhydryl compounds, such as DTT and glutathione. These chemicals are a synthetic and a physiological –SH containing reducing agents, respectively. All the experiments were performed under anaerobic conditions to avoid the re-oxidation of FAD cofactor by molecular oxygen. AIF was incubated at 25 °C with 2 mM DTT in the presence of both CHCHD4 and NAD^+. By monitoring FAD absorption spectra at different time intervals, it was possible to observe the progressive reduction of AIF FAD prosthetic group, as shown in Fig. 3.11 (A). Control experiments with the single interactors proved that AIF reduction occurs only in presence of both ligands. The same experiment was then performed with N-terminal peptide and either 2 mM DTT (Fig. 3.11 (B)) or 10 mM glutathione as reducing agents. In both cases FAD cofactor is reduced in presence of both the peptide and NAD^+, although at a lower rate when glutathione is the reductant.

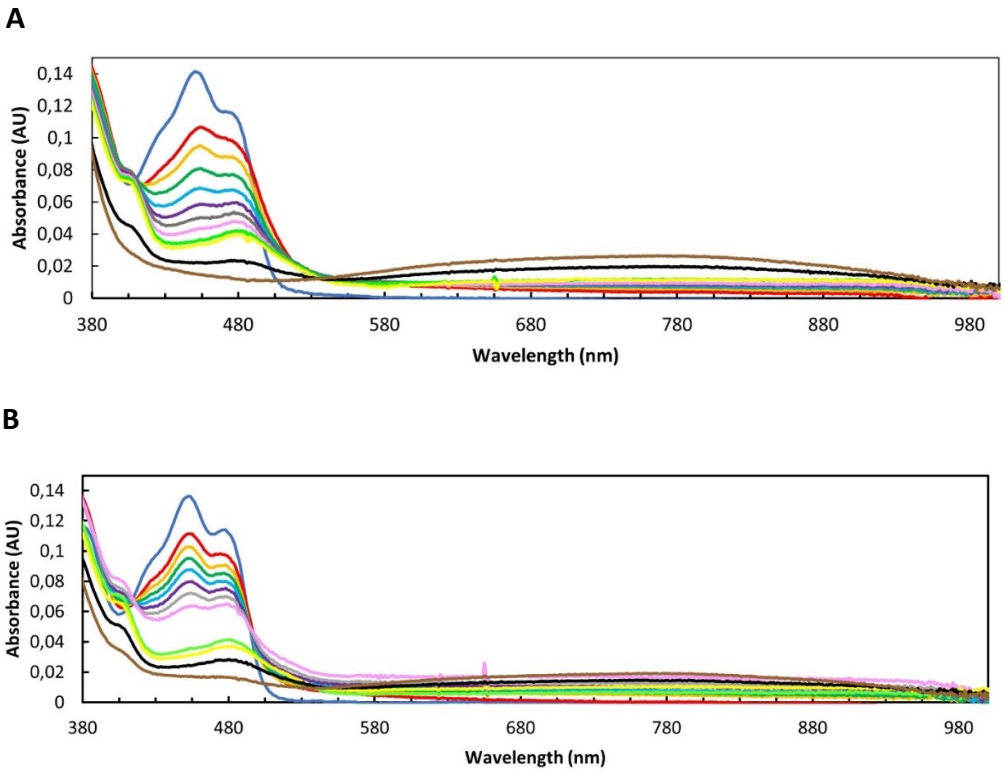

Fig. 3.11 Progress of AIF reduction by DTT in presence of CHCHD4 or its peptide and NAD^+. (A) The AIF absorption spectrum in presence of CHCHD4 (blue) was monitored over time after the addition of 7 mM NAD^+, in 50 mM Tris-HCl pH 8.0, 2 mM DTT buffer. The spectra were recorded after 3 min (red), 18 min (orange), 35 min (green), 50 min (light blue), 70 min (violet), 101 min (grey), 122 min (pink), 210 min (light green), 257 min (yellow), overnight (dark blue) and 5 days (brown). (B) The reduction of AIF by DTT was monitored over time also in presence of NAD^+ and the N-terminal peptide of CHCHD4. The spectra of AIF were recorded in presence of the peptide alone (blue) and after an incubation with NAD^+ of 2 min (red), 24 min (orange), 38 min (green), 53 min (light blue), 73 min (violet), 98 min (grey), 148 min (pink), 390 min (light green), overnight (yellow), 2 days (dark blue) and 5 days (brown).

The time course of spectral changes displays the same pattern with both reductants, although with different rates. The process is essentially biphasic: a faster phase, completed within a few hours in the case of DTT, and a much slower one evolving over several days. During the first phase, the oxidised FAD cofactor is converted to a species with an absorption maximum at about 480 nm. In the second phase, instead, this species is transformed to a final one with a wide absorption band extending from 500 to 900 nm. The intermediate species can be interpreted as the anionic form of the FAD semiquinone (one-electron reduced), while the final species as the FAD hydroquinone (two-electron reduced) in charge transfer complex with NAD^+. Since thiols are oxidised to disulfides with the transfer of an electrons pair, it is not obvious how the FAD semiquinone accumulates before the fully reduced FAD. This kinetics can be explained through the mechanism shown in Fig. 3.12.

$$FAD_{ox} + DTT_{red} \rightarrow FAD_{red} + DTT_{ox}$$

$$FAD_{red} + FAD_{ox} \rightleftharpoons 2FAD_{sq}$$

Fig. 3.12 Mechanism of the reaction of FAD reduction by DTT. The three FAD forms are the oxidised (ox), fully reduced (red) and semiquinone species (sq).

The first step is irreversible and slower than the second one, whose equilibrium is strongly shifted to the semiquinones. Consequently, as FAD is reduced receiving two electrons from DTT, it quickly reacts by single-electron transfer with oxidised FAD, generating its semiquinone species, which thus accumulates. Reduced FAD can appear only when the concentration of oxidised FAD becomes low enough to reverse

the equilibrium of the second step. Due to the presence of NAD^+, the CT complex between reduced FAD and NAD^+ is generated.

All these analyses demonstrated that, in the presence of either CHCHD4 or its N-terminal peptide, AIF becomes able to catalyse hydride transfer between sulfhydryl containing chemicals and FAD cofactor, that once reduced interacts with NAD^+ forming the CT complex. Further experiments are required to clarify the underlying molecular mechanism of the physiological role of AIF-CHCHD4 in assisting the oxidative folding of disulfide-containing polypeptides.

3.6 Characterization of AIF-CHCHD4 complex

3.6.1 Size Exclusion Chromatography (SEC) analysis of AIF-CHCHD4 complex

Once assessed the effect of CHCHD4 binding on the reactivity of the AIF active site, we decided to further investigate the binding process. We performed analytic SEC analyses of oxidised AIF in absence and in presence of CHCHD4. The experiments were conducted both at room temperature and at 10 °C to check the temperature dependence of complex stability. When present, CHCHD4 was at a molar ratio of either 1:1 and 2:1 with respect to of AIF. Samples were pre-incubated for 1 hour at 4 °C, before loading.

At room temperature, mixtures of AIF and CHCHD4 yielded two distinct peaks with retention of 8.9 ml and 9.7 ml, respectively, corresponding to the elution volume of AIF and CHCHD4, respectively (Fig. 3.13 (A)). This result demonstrated that at RT the complex fully dissociates during the separation process. On the contrary, at 10 °C an additional peak at about 13.8 ml (in this case an analytic Superdex 200 has been

used) was observed, corresponding to an apparent molecular weight of about 72 KDa, which approximately matches the sum of the masses of the two individual proteins. Even if peaks corresponding to both free AIF and free CHCHD4 remain visible (at 14.4 ml and 14.6 ml, respectively), at lower temperatures the dissociation of the complex is significantly slower than the separation time (Fig. 3.13 (B)). These findings, therefore, suggest that AIF and CHCHD4 interact as homodimer and that their dissociation is significantly hampered at low temperature. This important information proved to be useful especially in setting the crystallisation conditions, as reported below.

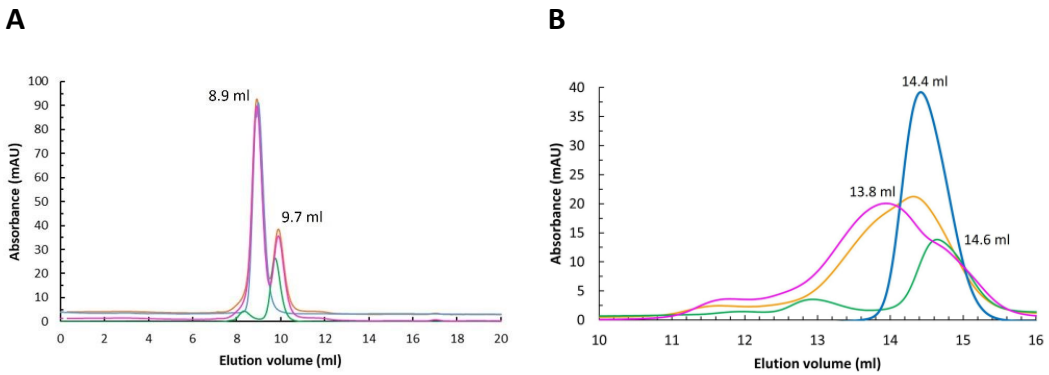

Fig. 3.13 Analytic SEC experiments on AIF-CHCHD4 interaction. (A) Superposed chromatograms of oxidised AIF (blue), oxidised AIF in presence of CHCHD4 in ratio 1:1 (orange) and 1:2 (pink), and CHCHD4 alone (green), at room temperature using an analytic Superdex 75 column. (B) Superposed chromatograms of AIF in complex with CHCHD4 at ratios 1:1 and 1:2 (orange and pink), and single protein alone (blue for AIF and green for CHCHD4), at 10 °C using an analytic Superdex 200 column. Elution volumes are reported close to the corresponding peak.

3.6.2 Effect of CHCHD4 binding on AIF conformational stability

Since SEC analysis demonstrated that AIF and CHCHD4 form a stable complex, we decided to investigate the effect of CHCHD4 binding on the conformational stability of AIF, both in its oxidised and reduced states by the ThermoFAD technique (65). As shown by the denaturation profiles displayed in Fig. 3.14 (A), CHCHD4 binding significantly destabilises oxidised AIF, whose melting temperature resulted 10 °C lower. The CT complex formation, upon NADH binding, causes important conformational changes which destabilise AIF, with a decrease of T_m from 73 °C to 57 °C. Interestingly, no effect of CHCHD4 binding on the thermal stability of AIF was detected when it was in the reduced/dimeric state. This result suggests that, while CHCHD4 binding induces a large conformational rearrangement on monomeric AIF, it leaves the structure of the dimeric form of the protein essentially unaffected (Fig. 3.14 (B)). The denaturation profile of oxidised AIF was also measured in the presence of NAD^+. Surprisingly, a destabilisation of the protein melting temperature, similar to that of NADH binding, was observed although no interactions were expected. This finding can be interpreted in terms of the ability of oxidised AIF to bind NAD^+ even in the absence of CHCHD4. However, such interaction induces no spectral change of the FAD cofactor (unproductive binding), as observed in spectrophotometric analyses. However, the addition of CHCHD4 enhances the destabilisation of AIF by NAD^+ by 10 °C, suggesting that CHCHD4 binding affects the structure of the AIF active site, allowing the stacking interaction between NAD^+ and oxidised FAD (productive binding).

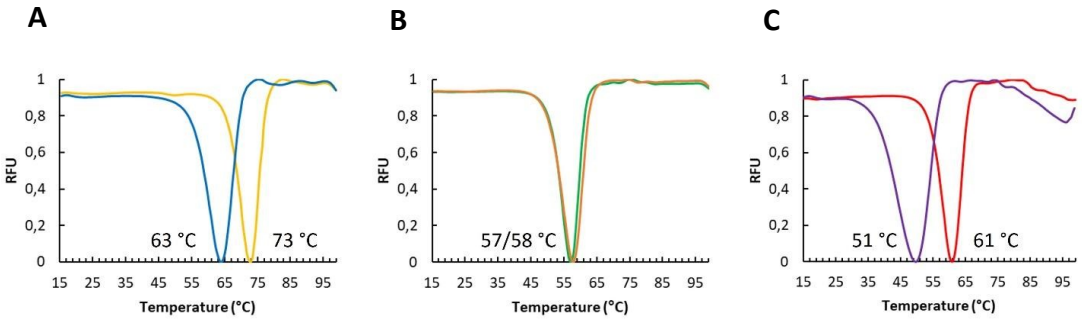

Fig. 3.14 Effect of CHCHD4 binding on AIF conformational stability. (A) Thermal denaturation profiles of oxidised AIF alone and with CHCHD4 are represented in yellow and blue, respectively. (B) Thermal denaturation profiles of reduced AIF alone and in complex with CHCHD4 are represented in orange and green, respectively. (C) Thermal denaturation profiles of oxidised AIF and NAD^+ in absence and in presence of CHCHD4 are represented in red and violet, respectively.

3.6.3 Microscale thermophoresis (MST) experiments on labelled-AIF titrated with CHCHD4/peptide

After the qualitative effects of CHCHD4 binding on the properties of the AIF active site were ascertained, the strength of such interaction was measured on a quantitative basis by means of the Microscale Thermophoresis (MST). This technique is based on the analysis of the alteration of the fluorescence emitted by a labelled target protein induced by temperature as a function of ligand concentration. The phenomenon that allows the observation of the fluorescence change is the thermophoresis: the induced motion of particles placed in a temperature gradient. In MST, such gradient is applied so that any types of binding-induced changes of molecular properties (charge, size, hydration shell or conformation), resulting in relative changes of sample motility, can be used to determine the binding affinity. In

our case, we labelled AIF at its C-terminal His-tag (a site whose modification is expected to have no effect on the conformation of the protein) through a non-covalent linkage. Then, we titrated the labelled AIF both in its oxidised and reduced states with either CHCHD4 or its N-terminal peptide. As already mentioned, the removal of the His-tag from CHCHD4 was required to avoid any interference with the label of AIF. Oxidised AIF and CHCHD4 interaction did not induce fluorescence quenching, while it was clearly detected a ligand dose-dependent thermophoresis effect from the recorded MST traces. The interpolation of MST data resulted in a K_d of 13 ± 2 µM. The same result was obtained also for oxidised AIF titrated with N-terminal peptide, with a K_d estimation of 15 ± 5 µM.

The experiments were then repeated after a 1 hour preincubation of AIF with a NADH excess, to obtain the reduced/dimeric form of the protein. In this case, the titration with CHCHD4 showed a significant variation of fluorescence emission in the capillary scan, suggesting a change in the fluorophore environment induced by the protein-protein interaction. To verify this hypothesis, we performed an EDTA/His6-peptide (ECP) control test, according to manufacturer instructions. The control experiment comprises two sub-tests: a control peptide test that verifies the interaction of the ligand with the His-tag bound tris-NTA dye, and an EDTA test that checks ligand-induced aggregation or adsorption to labware. Since initial fluorescence changes were not detected in both the control experiments, a CHCHD4-specific effect on AIF fluorescence emission upon binding was confirmed. Therefore, the raw fluorescence variation recorded during the capillary scan was exploited for data interpolation, even if CHCHD4 binding also induced a significant thermophoretic effect. A K_d value of 85 ± 15 nM was yielded for reduced AIF-CHCHD4 complex, around 150-fold lower than the K_d estimated for oxidised AIF. Repeating the experiment with the N-terminal peptide, we did not observe any

variation of AIF initial fluorescence and the binding affinity was estimated by the analysis of thermophoretic effect as 76 ± 2 nM.

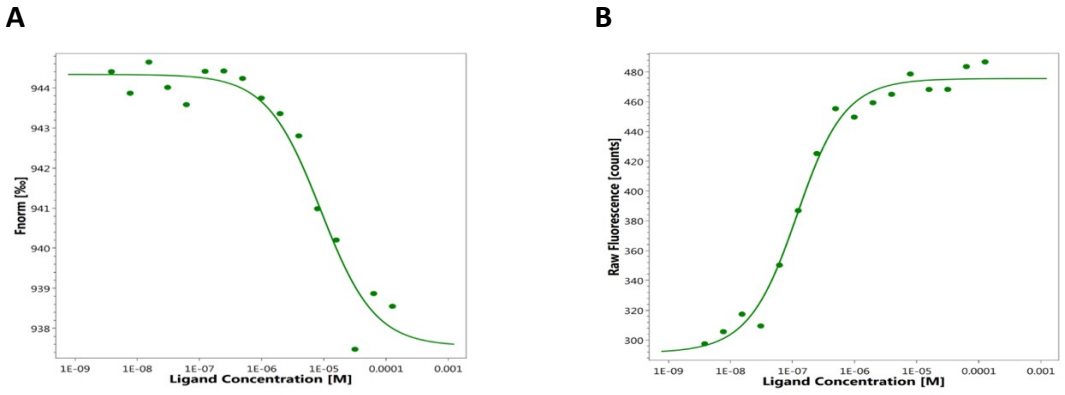

Fig. 3.15 Microscale Thermophoresis experiments on AIF in complex with CHCHD4. (A) Interpolation of MST fluorescence data of oxidised AIF titrated with CHCHD4, from which a K_d of 13 ± 2 µM was estimated. (B) Interpolation of initial fluorescence data of reduced AIF titrated with CHCHD4, from which a K_d of 85 ± 15 nM was estimated.

3.6.4 Isothermal Titration Calorimetry (ITC) analyses on AIF in presence of CHCHD4 peptide

The thermodynamics of the complex between AIF and the N-terminal peptide of CHCHD4 was studied through Isothermal Titration Calorimetry (ITC). I performed the experiments at the Institute of Biocomputation and Physics of Complex Systems (BIFI), University of Zaragoza (Spain) using the Auto-iTC200 instrument. ITC is a physical technique which allows the determination of thermodynamic parameters of interactions in solution as binding affinity (K_a), enthalpy variation (ΔH) and binding stoichiometry (N). During the experiments, the protein in the sample cell is titrated with the ligand, through a series of equal volume injections.

Since the ligand binding produces heat, the analysis consists in the measurements of the time-dependent input of power required to maintain the same temperature of the sample and the reference (filled with buffer) cells (66). In our case, we performed ITC experiments at 25 °C using either oxidised or reduced AIF (10 µM) in the sample cell (400 µl), titrated with 19 injections of 2 µl each of the peptide at the initial concentration of 100 µM. No signals of binding were detected between oxidised AIF and the peptide, while for the reduced AIF we estimated a K_a of 3.2 ± 0.2 μM^{-1} (K_d = 0.3 µM) and a ΔH of -12.4 ± 0.1 kcal/mol (TΔS = 3.5 kcal/mol, ΔG = -8.9 kcal/mol).

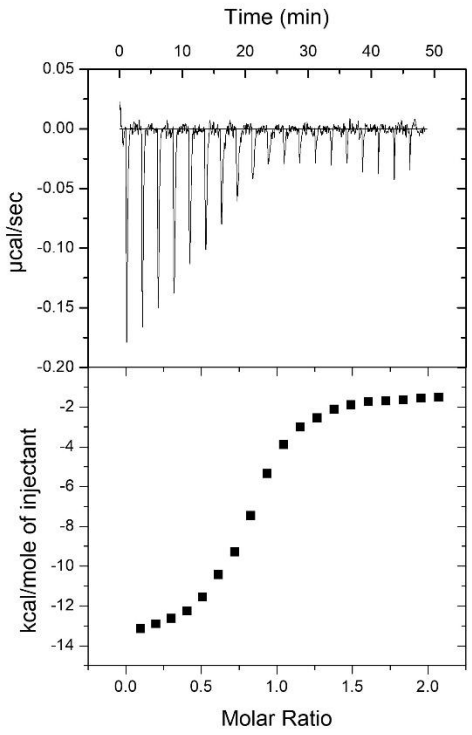

Fig. 3.16 ITC measurements of reduced AIF in presence of CHCHD4 N-terminal peptide. Raw data (top) and integrated normalised data (bottom) for titration of reduced AIF with the peptide.

3.7 Structural analyses of AIF and CHCHD4 interaction

3.7.1 AlphaFold model of AIF-CHCHD4 complex

For the structural investigation of AIF and CHCHD4 interaction, a model of the complex was built through ColabFold, based on AlphaFold2 prediction strategy (67). Given the FASTA sequences of the two proteins, MMseqs2 (Many-against-Many sequence searching) server performs diverse MSAs (Multiple Sequence Analysis) to find templates in two databases, UniRef100 and an environmental set of sequences. The latter is searched starting from the sequence profile generated by UniRef100 search as input. For complex prediction, the server performs both paired and unpaired MSAs: to solve the inter-chain interactions it selects the best hits within the same species, then it performs distinct MSAs, one for each protein, to guide the best structure prediction. The program, then, shows the top predicted models, ranked by quality scores. In the case of the AIF and CHCHD4 complex, the interaction is primarily mediated by the N-terminal portion of CHCHD4, as expected. Interestingly, the latter, which in the NMR structure does not adopt any secondary structure, is predicted to fold in two antiparallel β strands interacting with the C-terminal domain of AIF. In particular, the β hairpin formed by CHCHD4 interacts with the AIF strand containing residues 503-507. Since in the NMR structure this CHCHD4 portion is missed because it is probably disordered, the hypothesis is that its folding is induced by the binding to AIF. Prediction errors in AlphaFold models are expressed through pLDDT (predicted Local Distance Difference Test) and PAE (Predicted Alignment Error) parameters. pLDDT scores show the per-residue confidence: values higher than 90 indicate high confidence, while values under 50 indicate low confidence. In the five best predicted models of AIF-CHCHD4 complex the pLDDT are > 80 for most of the structure, except for N- and C-terminal residues and the portion corresponding to the C-terminal loop of AIF which have pLDDT values under 50. Also

the C-terminal part of CHCHD4 shows very low confidence values, further evidence that the N-terminal portion is the one most extensively involved in binding to AIF. Predicted aligned error (PAE), instead, gives a distance error for every pair of residues with a value range going from 0 to 30 Å. Values under 5 (represented in blue) indicate high confidence. The analysis of these quality scores, for each of the five models, confirms what already found with pLDDT estimation.

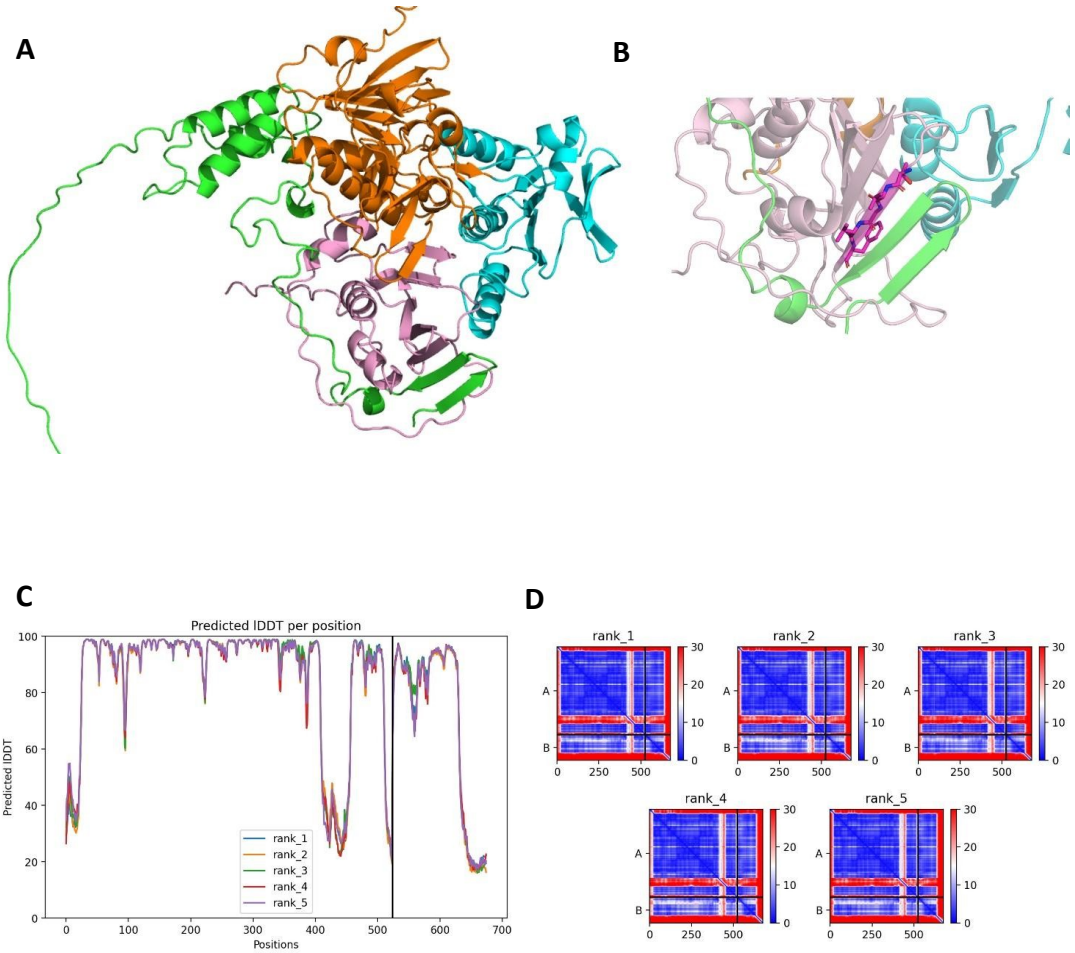

Fig. 3.17 Structure of AIF-CHCHD4 complex predicted by ColabFold. (A) Representation of AIF model in complex with CHCHD4, in cartoon drawing method. AIF FAD- and NADH-binding domains and C-terminal domain are represented in orange, cyan and pink,

respectively, while CHCHD4 is shown in green. (B) More detailed image of CHCHD4 N-terminal portion binding site on AIF C-terminal domain. Residues of the AIF β strand involved in the interaction (503-507) are represented as sticks and coloured in violet. (C) pLDDT and (D) PAE quality scores of the first 5 ranked models.

3.7.2 Mass spectrometry analysis on cross-linked AIF-CHCHD4 complex

The interaction between AIF and CHCHD4 was further characterised by mass spectrometry analyses on their cross-linked complex. AIF (27 µM) and CHCHD4 (40 µM) were incubated with 2 mM BS3 (bis-sulfosuccinimidyl-suberate) cross-linker, which reacts with primary amines forming stable amide bonds with the release of N-hydroxysulfosuccinimide. The reaction was stopped at different time intervals by addition of an excess of Tris to quench the cross-linker and the cross-linking products analysed on SDS-PAGE electrophoresis gels. As shown in Fig. 3.18 (A), even after a short incubation time of 5 minutes, we obtained two additional bands: one at 76 KDa, corresponding to the expected molecular weight of the heterodimeric complex between AIF and CHCHD4, and a broad one between 130 and 150 KDa. As control experiments, we incubated the single proteins with BS3. While for AIF two bands were observed, corresponding to the monomeric (57 KDa) and dimeric (120 KDa) forms of the protein, for CHCHD4 no evidence of oligomerization is present. The bands corresponding to cross-linked heterodimeric AIF-CHCHD4 complex obtained after 15 and 30 minutes of incubation with BS3 were then analysed by mass spectrometry. The experiments revealed the presence of a covalent interaction between the N-terminal amine of CHCHD4 and Lys517 residue of AIF. Interestingly, this lysine residue is located on the C-terminal loop (residues 508-562), confirming the binding region at the level of the C-terminal domain of AIF. As shown in Fig. 3.18 (B), in the AlphaFold model, the two cross-linked residues are at a distance of 28 Å,

higher than BS3 length, due to the closed conformation of the C-loop. However, given the low confidence values of this protein portion, probably the loop adopts another arrangement when oxidised AIF is bound to CHCHD4. Further mass spectrometry analyses were also performed on the bands corresponding to a molecular weight between 130 and 150 KDa and obtained after an incubation of 15 and 30 minutes with BS3. The results showed an additional cross-link between Lys133 residue of CHCHD4 and Lys277 residue of AIF. The presence of this covalent interaction promotes the formation of heterotrimers (130 KDa) and/or heterotetramers (150 KDa) of AIF-CHCHD4 complex.

A

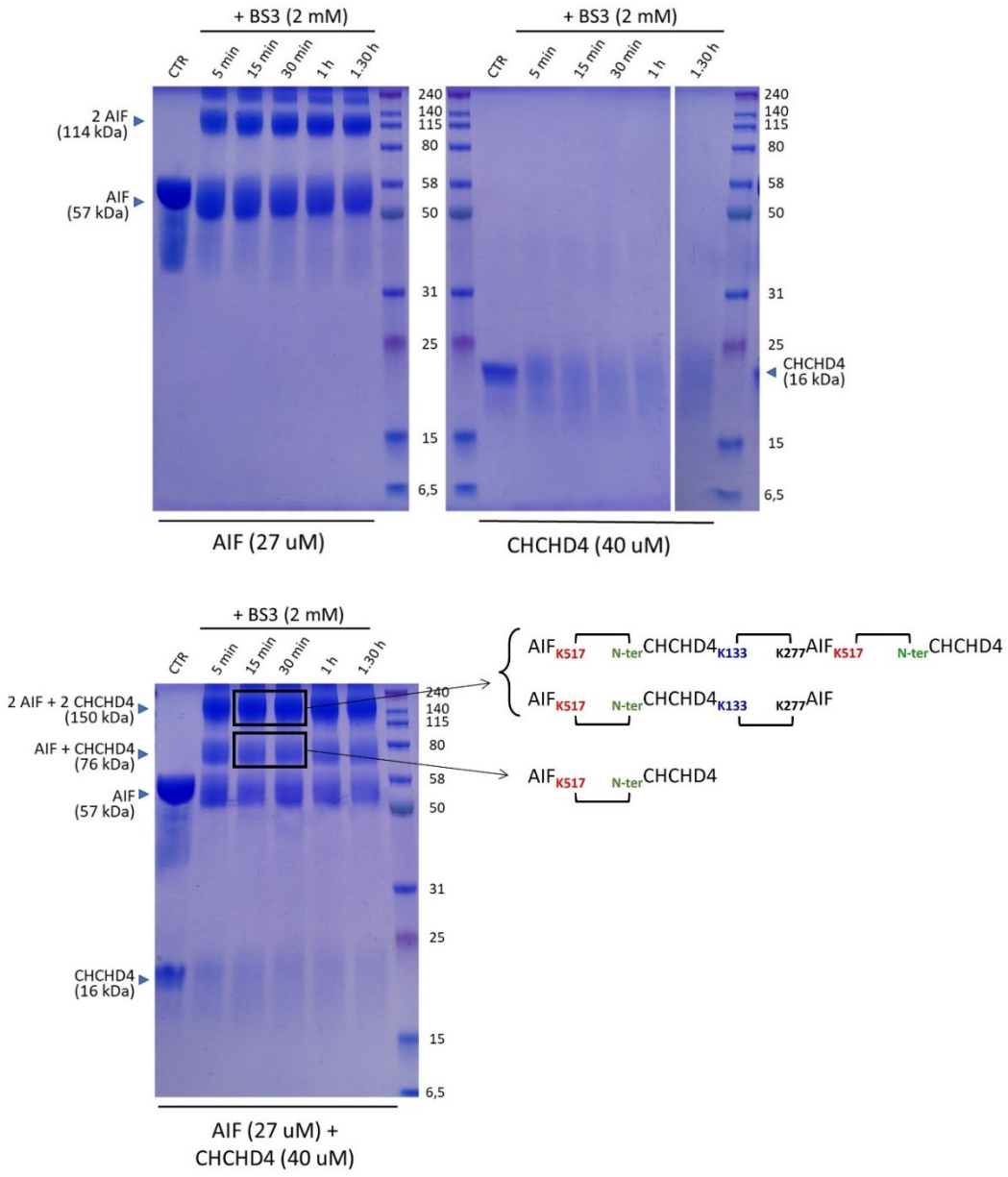
+ BS3 (2 mM)
+ BS3 (2 mM)
CTR
5 min
15 min
30 min
1 h
1.30 h
2 AIF (114 kDa)
AIF (57 kDa)
240
140
115
80
58
50
31
25
15
6,5
CHCHD4 (16 kDa)
AIF (27 uM)
CHCHD4 (40 uM)
2 AIF + 2 CHCHD4 (150 kDa)
AIF + CHCHD4 (76 kDa)
CHCHD4 (16 kDa)
AIF (27 uM) + CHCHD4 (40 uM)
AIF K517 N-ter CHCHD4 K133 K277 AIF K517 N-ter CHCHD4
AIF K517 N-ter CHCHD4 K133 K277 AIF
AIF K517 N-ter CHCHD4

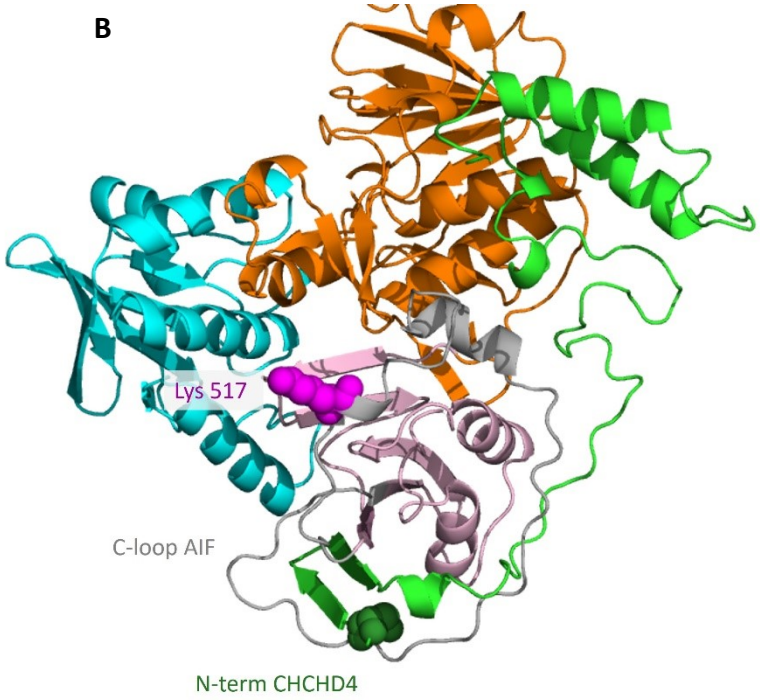

Fig. 3.18 Cross-linking experiments on AIF and CHCHD4 complex. (A) SDS-PAGE analyses of AIF, CHCHD4 and the mixture containing both proteins incubated with 2 mM BS3 cross-linker at different incubation times. CTR line corresponds to the proteins without BS3. The bands analysed by mass spectrometry are highlighted and the corresponding results showed. (B) Cartoon representation of AlphaFold predicted model of AIF and CHCHD4 complex, in which the N-terminal amine of CHCHD4 (dark green) and Lys517 (purple) are pictured as spheres. The C-loop of AIF is shown in grey.

3.7.3 Crystal structure of AIF in presence of CHCHD4 peptide

Experimental evidence of CHCHD4 binding site on AIF was achieved through the determination of the structure of the complex by X-ray crystallography. The crystallisation conditions were set up starting from the finding that AIF complexation

with CHCHD4 or its N-terminal portion, in presence of NAD^+, is highly favoured at low temperatures. Therefore, the crystallisation trials were performed at 4 °C by sitting drop, starting from a mixture of 210 µM oxidised AIF in presence of both the peptide and NAD^+ at a concentration of 1 mM and 9 mM, respectively. The crystals obtained were immersed in a cryoprotectant solution, similar to crystallisation condition but containing 25% glycerol and frozen in liquid nitrogen. Data collection was performed at ESRF (European Synchrotron Radiation Facility in Grenoble, France), beamline ID30A-1. Although the majority of tested crystals showed very low propensity to diffract, we were able to collect a dataset at 3.2 Å resolution. After data processing with autoPROC toolbox (68), the structure was solved by molecular replacement using as model the structure of murine reduced AIF (PDB: 3GD4). In the crystal asymmetric unit (a.u.) four copies of NAD^+-bound AIF were positioned and refined. After few cycles of refinement an additional electron density near AIF β strand 503-507 was observed for all the copies in the asymmetric unit, even though with inhomogeneous quality, and modelled with the N-terminal peptide. The structure of the complex was manually rebuilt with the Coot program (69) and extensively refined through Refmac5 (70,71), Phenix (72) and Buster (73). The overall structure of AIF is more similar to the reduced form of the protein (0.91 Å rmsd.) than the oxidised one (1.18 Å rmsd.). The N-terminal 27-mer peptide of CHCHD4 was modelled from residue Met1 or Thr3 to His20 or Lys25, depending on the electron density quality. As already predicted by AlphaFold, most of the peptide folds in a β hairpin composed of 2 antiparallel β strands (β1 and β2), with flexible N and C-terminal ends. The strands β1 (Cys4-Glu7) and β2 (Asp10-Phe14) are connected by the β turn (Gly8-Lys9) and stabilised by the salt bridge between Lys9 and Asp10. The complex formation is mediated by peptide β2 strand which binds to the AIF β sheet at its C-terminal domain, elongating it. In particular, the interaction is favoured by Asp10 of β2 strand forming an H-bond with the side chain of AIF

Thr503 and by hydrophobic interactions. AIF residues Tyr346, Phe507 and Tyr559 stabilises peptide Ile12 and Phe14 in a hydrophobic cleft, and Val504 and Val506 are in contact with Ile13 of β2 strand.

In all the four copies of AIF in the a.u. of our structure, ~22 residues at N- and C-terminal parts are missing. Moreover, the larger part of the C-loop was not modelled indicating a higher conformational flexibility of this protein portion in presence of the peptide. This observation supports the idea that CHCHD4 binding promotes the rearrangement of the C-terminal loop of AIF. The C-loop displacement probably favours the covalent bond formation, found in the cross-linked complex, between Lys517 and the N-terminal end of CHCHD4. Moreover, the analysis of AIF and the N-term peptide proved that CHCHD4 binding promotes the entrance of NAD^+ in the active site of AIF with the formation of a stacking interaction with the FAD prosthetic group, as already hypothesised after ThermoFAD experiments.

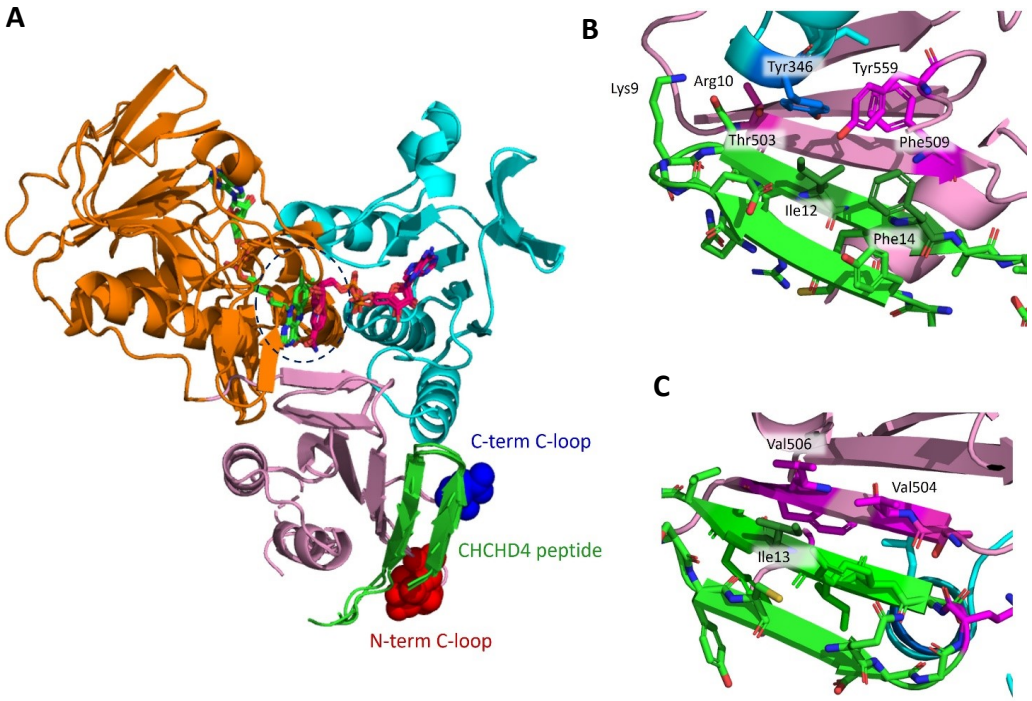

Fig. 3.19 Crystal structure of NAD-bound AIF in complex with CHCHD4 N-terminal peptide. (A) Cartoon representation of the four superposed copies of AIF in complex with the peptide (green). The N- and C-terminal visible parts of the C-loop are shown as spheres and coloured in red and blue, respectively. The dotted black circle highlights the parallel disposition of isoalloxazine of FAD (green, stick) and NAD^+ nicotinamide ring (violet, stick). (B-C) Stick representation of residues of both AIF and CHCHD4, responsible for the stabilisation of their interaction.

3.8 Validation of CHCHD4 binding site through mutagenesis experiments

3.8.1 AIF triple mutant T503D/V504K/G505P production

The structural characterization of the AIF-CHCHD4 complex identified AIF β strand 503-507 as the binding region of the N-terminal portion of CHCHD4. In order to validate the binding site, oligonucleotide-directed mutagenesis experiments were performed to substitute residues Thr503, Val504 and Gly505 with Asp, Lys and Pro, respectively. In particular, T503D and V504K substitutions were expected to cause electrostatic repulsion with N-peptide β2 strand Asp10 and Arg11, while G505P was supposed to alter the AIF β strand conformation and to disfavour the H-bond with Arg11. The triple mutant was obtained by using the expression vector containing the wild type coding sequence fused with a C-terminal His-tag, as template (pKK-AIFΔ101). In particular, we used the Q5® Site-Directed Mutagenesis Kit (New England BioLabs) with oligonucleotide primers specifically designed with the NEBaseChanger (New England BioLabs) design tool. AIF mutant was produced in recombinant form and purified according to the protocols already set up for the wild type protein: it consists of protein overexpression in *E. coli* BL21(DE3) cells, cell disruption to obtain the crude extract, a capturing step based on Ni-affinity chromatography and a final polishing step consisting of anion-exchange chromatography. All chromatographic steps were performed using an ÄKTA-FPLC system (GE Healthcare). T503D/V504K/G505P mutant was purified with a yield of about 2 mg of mutated protein per 1 L of cell culture, approximately 10-fold lower than that of wild type form, but still with high purity and without any changes in the elution profiles. Moreover, the FAD absorption spectrum of the mutant, compared to the wild type one, was not affected by the mutation.

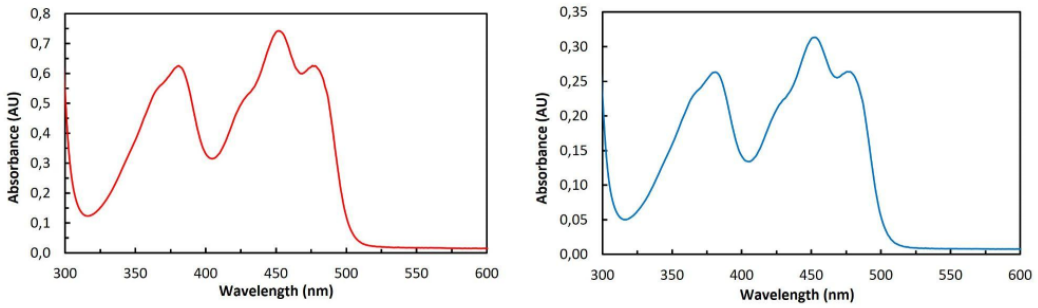

Fig. 3.20 Absorption spectrum of purified AIF triple mutant T503D/V504K/G505P (left) compared to that of WT AIF (right).

3.8.2 Characterization of the binding between CHCHD4 and the AIF mutant

The T503D/V504K/G505P AIF triple mutant was tested by different biophysical techniques, to prove the involvement of mutated residues in the interaction with CHCHD4 and, therefore, the AIF binding region identified in our structural studies on the complex. Firstly, we performed ThermoFAD experiments with oxidised/reduced AIF mutant in absence and in presence of CHCHD4. The three substitutions slightly alter the folding stability of both oxidised and reduced AIF, with a reduction in the melting temperature of 3.5 °C and 5.5 °C, respectively. Unlike the oxidised wild type AIF, which in presence of CHCHD4 undergoes a T_m decrease of 10 °C, the AIF mutant T_m is not affected by CHCHD4, indicating a lack of interaction. Regarding reduced AIF mutant, instead, its denaturation profiles are not altered by CHCHD4, as also happens for the WT protein. We monitored the folding stability of oxidised AIF triple mutant in presence of both CHCHD4 and NAD^+, or with NAD^+ alone. Even in the case of T503D/V504K/G505P mutant we observed an effect of NAD^+ binding on the T_m (ΔT_m= –10 °C), but the addition of CHCHD4 does not enhance such destabilisation,

unlike what was observed for WT AIF. This finding further confirms that the mutated region of AIF is important for the binding with CHCHD4.

Sample	Tm	Sample	Tm
Oxidised AIF WT	73.0°C ± 0.5	**Oxidised AIF DKP**	69.5°C ± 0.5
Oxidised AIF WT + CHCHD4	63.2 °C ± 0.8	**Oxidised AIF DKP + CHCHD4**	68.5°C ± 0.5
Reduced AIF WT	57.0°C ± 0.5	**Reduced AIF DKP**	51.5°C ± 0.5
Reduced AIF WT + CHCHD4	58.0°C ± 0.5	**Reduced AIF DKP + CHCHD4**	51.5°C ± 0.5
Oxidised AIF WT + NAD^+	61.0°C ± 0.5	**Oxidised AIF DKP + NAD^+**	58.0°C ± 0.5
Ox AIF + NAD^+ + CHCHD4	51.0°C ± 0.9	**Ox AIF DKP + NAD^+ + CHCHD4**	62.5°C ± 0.5

Fig. 3.21 Melting temperatures (T_m) of oxidised and reduced AIF wild type or mutant in absence and in presence of different ligands.

The triple mutant was also tested in Microscale Thermophoresis experiments and compared with WT protein results. We titrated labelled oxidised/reduced AIF mutant with both CHCHD4 full length and its N-terminal peptide, and no evidence of binding was detected under any condition. As further confirmation of the lack of interaction between AIF mutant and CHCHD4, analytic gel filtration analyses were performed at 10 °C. In particular, we loaded on a Superdex 200 Increase column the two single proteins and a solution containing both oxidised AIF triple mutant and CHCHD4 at a ratio of 1:2, after one hour of incubation at 4 °C. The AIF mutant elutes at the same elution volume of the WT protein (14.2 ml), confirming the absence of protein folding and stability effects of amino acid substitutions. However, the elution profile of the mixture, containing the triple mutant and CHCHD4, does not show an additional peak corresponding to the complex, as observed for the wild type protein

at 13.8 ml. As shown in Fig. 3.22, it elutes in a single peak at 14.3 ml, including the peaks of individual proteins (14.2 ml for AIF and 14.6 ml for CHCHD4).

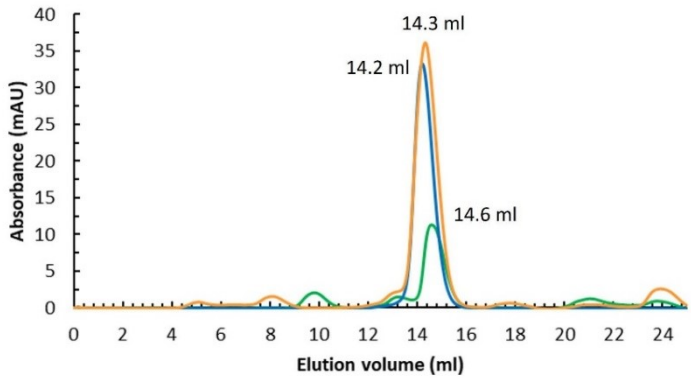

Fig. 3.22 Analytic SEC experiments on AIF DKP mutant and CHCHD4 interaction. Superposed chromatograms of oxidised AIF mutant (blue), CHCHD4 alone (green) and the mixture containing oxidised AIF mutant and CHCHD4 in ratio 1:2 (orange). The runs were performed at 10 °C using an analytic Superdex 200 Increase column. Elution volumes are reported close to the corresponding peak.

Finally, we repeated the cross-linking experiment on AIF mutant and CHCHD4, using 2 mM BS3 as cross-linker. SDS-PAGE electrophoretic gels showed the presence of a weak band at the molecular weight expected for the heterodimeric complex, but with an intensity much lower than that observed for WT AIF-CHCHD4 complex. Moreover, unlike wild type AIF, no bands corresponding to the heterotetrameric form of the complex are present. These results demonstrated once again that the β strand of AIF at its C-terminal domain is particularly important for binding to CHCHD4.

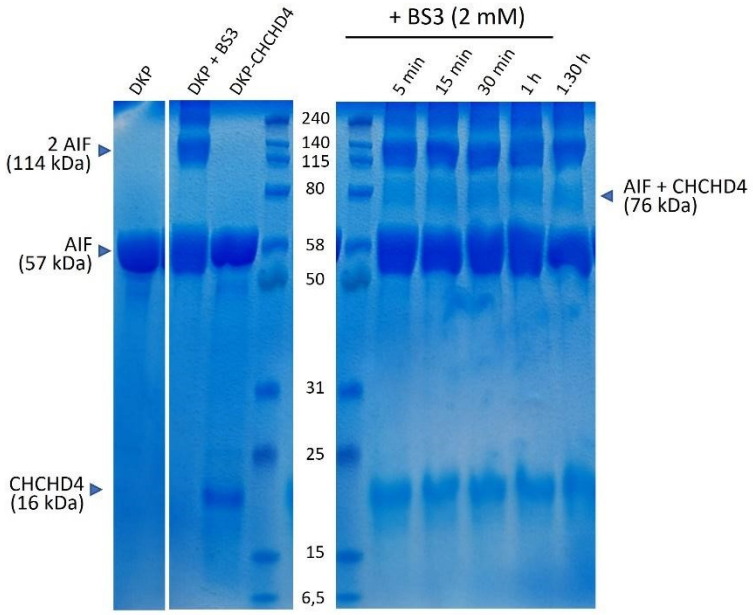

Fig. 3.23 Cross-linking experiments on AIF triple mutant in presence of CHCHD4. SDS-PAGE analysis of the mixture containing both AIF DKP and CHCHD4, after an incubation with 2 mM BS3 of 5, 15, 30, 60 and 90 minutes. "DKP", "DKP+BS3" and "DKP+CHCHD4" are control experiments with AIF mutant alone, AIF mutant with cross-linker, and AIF mutant in presence of CHCHD4 without BS3, respectively.

4. Conclusions and future perspectives

The presence of AIF and its direct interaction with CHCHD4, especially in its NADH-bound form, has been demonstrated to be essential for the correct folding and thus functionality of respiratory chain complexes, as well as their import inside the inter membrane space of mitochondria. Several diseases, mostly related to neurodegeneration, have been associated with AIF mutations or expression levels alterations, including impairments of its binding to CHCHD4. Since many properties of the AIF complex with CHCHD4 and its underlying molecular mechanisms are still not well characterised, in the present PhD project we focused on the functional and structural study of such complex.

The first step was to optimise the production and purification protocols of CHCHD4 full length, incrementing the protein yield and homogeneity. Then, the effect of CHCHD4 binding on AIF FAD microenvironment was evaluated, as well as the effect of its N-terminal peptide of 27 residues sufficient for AIF interaction. Both CHCHD4 full length (FL) and its peptide interact with oxidised AIF, showing FAD absorption spectrum perturbation with higher intensity for CHCHD4 FL. It can be argued that, although the peptide is self-sufficient to establish a stable contact, the rest of the protein is required to induce a full conformational transition in AIF. To test this hypothesis, the experiments could be repeated in presence of a CHCHD4 form lacking the N-terminal portion. Interestingly, while the binding and release of the peptide were found to be very fast, those of the whole protein turned out to be remarkably slow. The latter observation can be interpreted as a consequence of large conformational changes occurring before or after the binding. Once assessed the modulation of AIF active site upon ligand binding and the faster binding kinetic of the peptide, we studied how the active site reactivity of AIF is influenced by the presence of the peptide. In particular, we found that the peptide increments the

reductase activity of AIF by decreasing the K_m for NADH of about 20-folds and doubling the catalytic constant. Moreover, the enzymatic activation occurs with an apparent K_d of about 0.4 μM. Since the interaction increased the affinity of AIF for NADH, we hypothesised that it could similarly affect its affinity for NAD^+. In its oxidised monomeric state, AIF is known to be unable to bind NAD^+, however in the presence of CHCHD4 it becomes able to form a complex with the dinucleotide. The shape and intensity of the resulting difference absorption spectra are suggestive of a full occupancy of the active side by the nicotinamide ring with formation of a stacking interaction with the flavin ring system. As expected, the N-terminal peptide favoured NAD^+ binding to AIF at a lower extent. We concluded that the presence of CHCHD4 or its peptide affects the active site conformation of AIF, favouring the entrance of NAD^+ and its interaction with FAD cofactor. Furthermore, such effect turned out to be highly temperature sensitive. Through a temperature scanning experiment, we studied the dependence of AIF saturation on the temperature. Preliminary experiments suggested that the binding of NAD^+ is secondary to the interaction with the peptide and it is the latter to be affected by the temperature. Peptide and NAD^+ binding displays positive cooperativity and the interaction is improved at low temperature. Then, we discovered that CHCHD4 modulates the AIF reactivity, in the presence of NAD^+, towards thiol groups. This observation is particularly relevant, considering that the AIF-CHCHD4 complex has a prominent role in the mitochondrial disulfide relay system. Thiol compounds, like DTT and glutathione, are able to reduce AIF bound FAD, suggesting its accessibility to such compounds. The idea is that they form a transient covalent adduct with FAD, in order to be oxidised to disulfides. Considering that AIF is predominantly present in reduced forms inside mitochondria, it can be hypothesised that, if its thiol reactivity has any physiological implication, it could work in promoting the reduction of disulfides, rather than in their formation.

The next step was to characterise the interaction between AIF and CHCHD4 through various techniques, including analytic SEC, thermal denaturation, thermophoresis and calorimetry. In particular, we found that oxidised AIF and CHCHD4 form a heterodimer highly stable at low temperatures, with a dissociation time slower than elution time. The presence of CHCHD4 influences oxidised AIF thermal stability, causing the decrease of its melting temperature of about 10 °C. On the contrary, the reduced form of the enzyme, which shows a ΔT_m of -16 °C respect to the oxidised form, is not affected by the presence of the ligand. These results suggest that CHCHD4 binding induces important structural conformational changes in oxidised AIF, equivalent to those observed for protein reduction. Furthermore, as already observed in spectrophotometric analyses on FAD spectrum, the presence of CHCHD4 favours the active positioning of NAD^+ in the active site of oxidised AIF. Through MST experiments, we further proved that the oligomerization state of AIF and the FAD microenvironment conformation influence CHCHD4 binding. Upon reduction, indeed, AIF acquires a 100-fold increased affinity for CHCHD4 or its peptide, which form a tight complex with AIF in its CT complex/dimeric state. These results were confirmed by ITC analyses, through which we also found that CHCHD4 binding is a spontaneous exothermic reaction.

The structural characterization of the complex allowed the identification of AIF binding site for CHCHD4. Despite in NMR experiments the N-terminal portion of CHCHD4 has shown to be unstructured, in our crystal structure it adopts a β hairpin conformation. According also to AlphaFold predicted model and cross-linking experiments, the C-terminal domain of AIF was identified as CHCHD4 binding site. In detail, the β2 strand of CHCHD4 10-14 was found to interact with AIF β strand 503-507, extending the C-terminal β sheet of the enzyme. Interestingly, in our crystal structure the C-loop seems to assume an open and solvent-exposed conformation,

which is also suggested by the formation of the covalent link between AIF Lys517 and CHCHD4 N-terminal portion, through BS3 cross-linker, found in mass-spectrometry analysis. This observation allows us to hypothesise a strong correlation between the state of the active site and the disposition of the C-loop. It is known that the formation of the CT complex, upon NADH interaction, induces conformational changes that start from the active site residues and lead to the opening of the C-loop. The results we obtained support this proposed allosteric pathway, also explaining the higher affinity of reduced AIF for CHCHD4. Interestingly, we also demonstrated the presence of an inverse correlation between the C-loop and the FAD binding site. As observed in thermal stability analyses and in our structural studies, the binding of CHCHD4 favours the opening of the C-loop, which in turn leads to the stacking interaction between NAD^+ and FAD cofactor in the active site, as also proven with spectrophotometric assays.

The identification of CHCHD4 binding site, as well as its bidirectional correlation with AIF redox state and effects on enzyme activity, represent important outcomes which shed light on AIF and CHCHD4 interaction properties. Nonetheless, further analyses are necessary to fully understand the mechanism of action of the complex in promoting oxidative folding of substrates. Future studies should focus on a better understanding of molecular properties of AIF physiopathology, in order to improve the chance to develop therapies for the growing number of AIF-related diseases.

5. Materials and methods

Materials and methods of most of the experiments described in the *Results and discussion* part are described in the submitted article, attached to this PhD thesis.

Spectrophotometric studies

All spectrophotometric procedures were carried out using a 8453 (Agilent) diode-array single beam spectrophotometer.

The extinction coefficient in the visible region of AIF was determined recording its absorption spectrum before and after denaturing the protein with 0.2% SDS. By quantitating the amount of FAD released by the unfolded protein (ε_{450}= 11.3 $mM^{-1}cm^{-1}$), its concentration was determined, thus allowing the calculation of the extinction coefficient, which was found to be 12.8 $mM^{-1}cm^{-1}$, in full agreement with published data.

Difference absorption spectrum of the AIF-CHCHD4/peptide complex - To evaluate the possible alteration of the structural features of the FAD microenvironment induced by CHCHD4 binding, the FAD absorption spectrum of AIF in the presence of a fixed concentration of the partner protein was determined. The spectrum of 12.1 µM AIF was measured in presence or absence of 25.4 µM CHCHD4, with an incubation of 30 min at 4 °C. The solutions were clarified by centrifugation at 13,000 rpm for about 10 minutes and spectra were recorded at 25 °C. The difference spectrum of the complex was computed by subtracting from the spectrum of the sample containing both AIF and CHCHD4 those with the two separated proteins. The experiments were performed under both low (50 mM Tris-HCl, pH 8.0, 2 mM DTT) and high (50 mM Tris-HCl, pH 8.0, 200 mM NaCl, 2 mM DTT) ionic strength. The same

analyses were performed with the peptide at a final concentration of 146 µM in the assay.

Kinetics of CHCHD4 binding to AIF - The evolution of the spectral properties of the FAD prosthetic group of AIF upon CHCHD4 addition was monitored following the absorbance variation at 487 nm, over 60 min at 25 °C on an incubation mixture containing 12.3 µM AIF and 25.4 µM CHCHD4, in 50 mM Tris-HCl, pH 8.0.

NADH-DCIP activity assay - The NADH–DCIP reductase reaction catalysed by AIF was studied under steady-state conditions at 25 °C in 100 mM Na-phosphate, pH 8.0. To estimate the kinetic parameters, 60.5 nM AIF was incubated in absence and in presence of 0.7 µM peptide, varying the concentration of NADH (between 0.1 and 1.4 mM in the experiment without the peptide and between 6 and 133 µM in the presence of the peptide), while keeping constant that of DCIP at 35.7 µM. The reactions were monitored spectrophotometrically at a wavelength of 600 nm, following DCIP reduction. All steady-state data, i.e., initial velocity values (v) as a function of the reductant concentration ([S]), were analysed using Grafit 4 (Erithacus Ltd) by nonlinear fitting.

To estimate the apparent dissociation constant of the AIF-peptide complex, the NADH-DCIP reductase activity of AIF was determined at a concentration of 100 µM NADH in the presence of increasing concentrations of the peptide between 60 nM and 1.98 µM. The apparent K_d of the AIF-peptide complex was estimated by fitting the increase in the reaction rate determined by the peptide as a function of its concentration with a quadratic equation by non-linear regression analysis using the software GraFit 4. The quadratic equation was based on the following relationship between saturation fraction ϑ and ligand concentration:

$$\theta = \frac{[AIF - peptide]}{[AIF]_{tot}}$$
$$= \frac{K_d + [peptide] + [AIF]_{tot} - \sqrt{(K_d + [peptide] + [AIF]_{tot})^2 - 4[AIF]_{tot}[peptide]}}{2[AIF]_{tot}}$$

AIF reactivity towards thiol groups – To evaluate CHCHD4 effect on AIF reactivity towards thiol-containing compounds, the FAD absorption spectrum of 10.4 µM AIF in presence of 21.8 µM CHCHD4 and 7 mM NAD^+ was recorded at 25 °C in 50 mM Tris-HCl, pH 8.0, 2 mM DTT. The analyses were performed under anaerobiosis conditions to avoid FAD re-oxidation by oxygen. The reaction progress was monitored measuring the spectra at different time intervals up to 5 days. Control experiments were performed with either NAD^+ or CHCHD4 alone at the same concentrations and maintaining the same experimental conditions.

The reactivity of NAD^+-bound AIF in complex with the peptide toward DTT or glutathione was also studied. The absorption spectrum of a solution containing 10.4 µM AIF, 100 µM CHCHD4 peptide and 7 mM NAD^+ was monitored at different times over 5 days, at 25 °C in 50 mM Tris-HCl, pH 8.0, and 2 mM DTT or 10 mM glutathione.

Analytic SEC

To evaluate the temperature dependence of AIF-CHCHD4 interaction stability, analytic SEC experiments on the complex were performed both at room temperature using a Superdex 75 HR 10/30 column and at 10 °C using a Superdex 200 Increase 10/300 GL. Solutions of 20 µM of wild type AIF were incubated for 1 h at 4 °C with 25 µM or 50 µM CHCHD4, to also study the molar ratio of AIF-CHCHD4 association. The elution profiles of the two proteins at the same concentrations were

also acquired at both temperatures. All experiments were performed in 50 mM Tris-HCl, pH 8.0, 200 mM NaCl, 5 mM DTT buffer at a flow rate of 0.5 ml/min. Analytic SEC analyses were performed also with AIF triple mutant in presence of CHCHD4 using a Superdex 200 Increase 10/300 GL column. A solution of 20 µM AIF mutant was incubated for 1h at 4 °C with 50 µM CHCHD4 and the separation was performed at 10 °C at a flow rate of 0.5 ml/min with Tris-HCl, pH 8.0, 200 mM NaCl, 5 mM DTT buffer.

Isothermal Titration Calorimetry

Calorimetry experiments were conducted in 50 mM Na-phosphate pH 7.4, at 25 °C, using the Auto-iTC200 instrument. For the thermodynamic characterization of AIF and N-terminal CHCHD4 peptide interaction, the peptide at 100 µM was injected into a sample cell containing 400 µl of oxidised or reduced AIF at 10 µM. Each experiment involved 19 injections of 2 µl. The integration details, as baseline and integration range, of the binding peaks were set up using Origin 7.0 software package (OriginLab). Thermodynamic parameters, such as N (number of sites), K (binding constant in M^{-1}), and ΔH (heat change in cal/mole) were calculated using the "one set of sites" fitting model. It works for any number of sites *n,* if all sites have the same K and ΔH.

References

1. Ghisla S, Massey V. Mechanisms of flavoprotein-catalyzed reactions. European Journal of Biochemistry. 1989;181(1):1–17.

2. Lienhart WD, Gudipati V, Macheroux P. The human flavoproteome. Archives of Biochemistry and Biophysics. 2013 Jul 15;535(2):150–62.

3. Northrop-Clewes CA, Thurnham DI. The Discovery and Characterization of Riboflavin. Annals of Nutrition & Metabolism. 2012;61(3):224–30.

4. Warburg O, Christian W. Isolation of the prosthetic group of d-amino-acid oxidase. Biochem Ztschr. 1938;298:150–68.

5. Susin SA, Lorenzo HK, Zamzami N, Marzo I, Snow BE, Brothers GM, et al. Molecular characterization of mitochondrial apoptosis-inducing factor. Nature. 1999 Feb 4;397(6718):441–6.

6. Novo N, Ferreira P, Medina M. The apoptosis-inducing factor family: Moonlighting proteins in the crosstalk between mitochondria and nuclei. IUBMB Life. 2021 Mar 1;73(3):568–81.

7. Klim J, Gładki A, Kucharczyk R, Zielenkiewicz U, Kaczanowski S. Ancestral State Reconstruction of the Apoptosis Machinery in the Common Ancestor of Eukaryotes. G3 Genes|Genomes|Genetics. 2018 Jun 1;8(6):2121–34.

8. Sevrioukova IF. Apoptosis-inducing factor: structure, function, and redox regulation. Antioxidants & redox signaling. 2011 Jun 15;14(12):2545–79.

9. Maté MJ, Ortiz-Lombardía M, Boitel B, Haouz A, Tello D, Susin SA, et al. The crystal structure of the mouse apoptosis-inducing factor AIF. Nature structural biology. 2002;9(6):442–6.

10. Senda T, Yamada T, Sakurai N, Kubota M, Nishizaki T, Masai E, et al. Crystal structure of NADH-dependent ferredoxin reductase component in biphenyl dioxygenase1 1Edited by D. Rees. Journal of Molecular Biology. 2000 Dec 1;304(3):397–410.

11. Sevrioukova IF. Redox-Linked Conformational Dynamics in Apoptosis-Inducing Factor. Journal of Molecular Biology. 2009 Jul 31;390(5):924–38.

12. Sorrentino L, Calogero AM, Pandini V, Vanoni MA, Sevrioukova IF, Aliverti A. Key Role of the Adenylate Moiety and Integrity of the Adenylate-Binding Site for the NAD+/H Binding to Mitochondrial Apoptosis-Inducing Factor. Biochemistry. 2015 Nov 4;54(47):6996–7009.

13. Villanueva R, Ferreira P, Marcuello C, Usón A, Miramar MD, Peleato ML, et al. Key Residues Regulating the Reductase Activity of the Human Mitochondrial Apoptosis Inducing Factor. Biochemistry. 2015 Aug 25;54(33):5175–84.

14. Ferreira P, Villanueva R, Martínez-Júlvez M, Herguedas B, Marcuello C, Fernandez-Silva P, et al. Structural Insights into the Coenzyme Mediated Monomer–Dimer Transition of the Pro-Apoptotic Apoptosis Inducing Factor. Biochemistry. 2014 Jul 1;53(25):4204–15.

15. Romero-Tamayo S, Laplaza R, Velazquez-Campoy A, Villanueva R, Medina M, Ferreira P. W196 and the *β*-Hairpin Motif Modulate the Redox Switch of Conformation and the Biomolecular Interaction Network of the Apoptosis-Inducing Factor. Oxidative Medicine and Cellular Longevity. 2021 Jan 15;2021:e6673661.

16. Wu CC, Bratton SB. Regulation of the Intrinsic Apoptosis Pathway by Reactive Oxygen Species. Antioxidants & Redox Signaling. 2013 Aug 20;19(6):546–58.

17. Czabotar PE, Lessene G, Strasser A, Adams JM. Control of apoptosis by the BCL-2 protein family: implications for physiology and therapy. Nat Rev Mol Cell Biol. 2014 Jan;15(1):49–63.

18. Joza N, Pospisilik JA, Hangen E, Hanada T, Modjtahedi N, Penninger JM, et al. AIF: not just an apoptosis-inducing factor. Annals of the New York Academy of Sciences. 2009;1171:2–11.

19. Ravagnan L, Gurbuxani S, Susin SA, Maisse C, Daugas E, Zamzami N, et al. Heat-shock protein 70 antagonizes apoptosis-inducing factor. Nat Cell Biol. 2001 Sep;3(9):839–43.

20. Wilkinson JC, Wilkinson AS, Galbán S, Csomos RA, Duckett CS. Apoptosis-Inducing Factor Is a Target for Ubiquitination through Interaction with XIAP. Molecular and Cellular Biology. 2008 Jan 1;28(1):237–47.

21. Kim JT, Kim KD, Song EY, Lee HG, Kim JW, Kim JW, et al. Apoptosis-inducing factor (AIF) inhibits protein synthesis by interacting with the eukaryotic translation initiation factor 3 subunit p44 (eIF3g). FEBS Letters. 2006 Nov 27;580(27):6375–83.

22. Collingwood TS, Smirnova EV, Bogush M, Carpino N, Annan RS, Tsygankov AY. T-cell Ubiquitin Ligand Affects Cell Death through a Functional Interaction with Apoptosis-inducing Factor, a Key Factor of Caspase-independent Apoptosis *. Journal of Biological Chemistry. 2007 Oct 19;282(42):30920–8.

23. Candé C, Vahsen N, Kouranti I, Schmitt E, Daugas E, Spahr C, et al. AIF and cyclophilin A cooperate in apoptosis-associated chromatinolysis. Oncogene. 2004 Feb;23(8):1514–21.

24. Artus C, Boujrad H, Bouharrour A, Brunelle MN, Hoos S, Yuste VJ, et al. AIF promotes chromatinolysis and caspase-independent programmed necrosis by interacting with histone H2AX. The EMBO Journal. 2010 May 5;29(9):1585–99.

25. Novo N, Romero-Tamayo S, Marcuello C, Boneta S, Blasco-Machin I, Velázquez-Campoy A, et al. Beyond a platform protein for the degradosome assembly: The Apoptosis-Inducing Factor as an efficient nuclease involved in chromatinolysis. PNAS Nexus. 2023 Feb 1;2(2):pgac312.

26. Hüttemann M, Lee I, Pecinova A, Pecina P, Przyklenk K, Doan JW. Regulation of oxidative phosphorylation, the mitochondrial membrane potential, and their role in human disease. J Bioenerg Biomembr. 2008 Oct 1;40(5):445–56.

27. Granata S, Dalla Gassa A, Tomei P, Lupo A, Zaza G. Mitochondria: a new therapeutic target in chronic kidney disease. Nutrition & metabolism. 2015 Nov 25;12:49.

28. Klein JA, Longo-Guess CM, Rossmann MP, Seburn KL, Hurd RE, Frankel WN, et al. The harlequin mouse mutation downregulates apoptosis-inducing factor. Nature. 2002 Sep;419(6905):367–74.

29. Churbanova IY, Sevrioukova IF. Redox-dependent changes in molecular properties of mitochondrial apoptosis-inducing factor. The Journal of biological chemistry. 2008 Feb 29;283(9):5622–31.

30. Pospisilik JA, Knauf C, Joza N, Benit P, Orthofer M, Cani PD, et al. Targeted deletion of AIF decreases mitochondrial oxidative phosphorylation and protects from obesity and diabetes. Cell. 2007 Nov 2;131(3):476–91.

31. Cheung EC, Joza N, Steenaart NA, McClellan KA, Neuspiel M, McNamara S, et al. Dissociating the dual roles of apoptosis-inducing factor in maintaining mitochondrial structure and apoptosis. The EMBO Journal. 2006 Sep 6;25(17):4061–73.

32. Vahsen N, Candé C, Brière JJ, Bénit P, Joza N, Larochette N, et al. AIF deficiency compromises oxidative phosphorylation. The EMBO Journal. 2004 Nov 24;23(23):4679–89.

33. Delavallée L, Mathiah N, Cabon L, Mazeraud A, Brunelle-Navas MN, Lerner LK, et al. Mitochondrial AIF loss causes metabolic reprogramming, caspase-independent cell death blockade, embryonic lethality, and perinatal hydrocephalus. Molecular Metabolism. 2020 Oct 1;40:101027.

34. Ishimura R, Martin GR, Ackerman SL. Loss of Apoptosis-Inducing Factor Results in Cell-Type-Specific Neurogenesis Defects. J Neurosci. 2008 May 7;28(19):4938–48.

35. Chacinska A, Pfannschmidt S, Wiedemann N, Kozjak V, Sanjuán Szklarz LK, Schulze-Specking A, et al. Essential role of Mia40 in import and assembly of mitochondrial intermembrane space proteins. The EMBO Journal. 2004 Sep 29;23(19):3735–46.

36. Hofmann S, Rothbauer U, Mühlenbein N, Baiker K, Hell K, Bauer MF. Functional and Mutational Characterization of Human MIA40 Acting During Import into the Mitochondrial Intermembrane Space. Journal of Molecular Biology. 2005 Oct 28;353(3):517–28.

37. Dickson-Murray E, Nedara K, Modjtahedi N, Tokatlidis K. The Mia40/CHCHD4 Oxidative Folding System: Redox Regulation and Signaling in the Mitochondrial Intermembrane Space. Antioxidants. 2021 Apr;10(4):592.

38. Banci L, Bertini I, Cefaro C, Ciofi-Baffoni S, Gallo A, Martinelli M, et al. MIA40 is an oxidoreductase that catalyzes oxidative protein folding in mitochondria. Nature Structural & Molecular Biology 2009 16:2. 2009 Feb 1;16(2):198–206.

39. Hangen E, Féraud O, Lachkar S, Mou H, Doti N, Fimia GM, et al. Interaction between AIF and CHCHD4 Regulates Respiratory Chain Biogenesis. Molecular cell. 2015 Jun 18;58(6):1001–14.

40. Meyer K, Buettner S, Ghezzi D, Zeviani M, Bano D, Nicotera P. Loss of apoptosis-inducing factor critically affects MIA40 function. Cell Death Dis. 2015 Jul;6(7):e1814–e1814.

41. Murschall LM, Gerhards A, MacVicar T, Peker E, Hasberg L, Wawra S, et al. The C-terminal region of the oxidoreductase MIA40 stabilizes its cytosolic precursor during mitochondrial import. BMC Biology. 2020 Aug 6;18(1):96.

42. Reinhardt C, Arena G, Nedara K, Edwards R, Brenner C, Tokatlidis K, et al. AIF meets the CHCHD4/Mia40-dependent mitochondrial import pathway. Biochimica et Biophysica Acta (BBA) - Molecular Basis of Disease. 2020 Jun 1;1866(6):165746.

43. Wischhof L, Scifo E, Ehninger D, Bano D. AIFM1 beyond cell death: An overview of this OXPHOS-inducing factor in mitochondrial diseases. eBioMedicine. 2022 Sep 1;83:104231.

44. Ghezzi D, Sevrioukova I, Invernizzi F, Lamperti C, Mora M, D'Adamo P, et al. Severe X-linked mitochondrial encephalomyopathy associated with a mutation in apoptosis-inducing factor. Am J Hum Genet. 2010 Apr 9;86(4):639–49.

45. Berger I, Ben-Neriah Z, Dor-Wolman T, Shaag A, Saada A, Zenvirt S, et al. Early prenatal ventriculomegaly due to an AIFM1 mutation identified by linkage analysis and whole exome sequencing. Molecular Genetics and Metabolism. 2011 Dec 1;104(4):517–20.

46. Ardissone A, Piscosquito G, Legati A, Langella T, Lamantea E, Garavaglia B, et al. A slowly progressive mitochondrial encephalomyopathy widens the spectrum of AIFM1 disorders. Neurology. 2015 May 26;84(21):2193–5.

47. Diodato D, Tasca G, Verrigni D, D'Amico A, Rizza T, Tozzi G, et al. A novel AIFM1 mutation expands the phenotype to an infantile motor neuron disease. Eur J Hum Genet. 2016 Mar;24(3):463–6.

48. Heimer G, Eyal E, Zhu X, Ruzzo EK, Marek-Yagel D, Sagiv D, et al. Mutations in AIFM1 cause an X-linked childhood cerebellar ataxia partially responsive to riboflavin. European Journal of Paediatric Neurology. 2018 Jan 1;22(1):93–101.

49. Morton SU, Prabhu SP, Lidov HGW, Shi J, Anselm I, Brownstein CA, et al. AIFM1 mutation presenting with fatal encephalomyopathy and mitochondrial disease in an infant. Cold Spring Harb Mol Case Stud. 2017 Jan 3;3(2):a001560.

50. Pronicka E, Piekutowska-Abramczuk D, Ciara E, Trubicka J, Rokicki D, Karkucińska-Więckowska A, et al. New perspective in diagnostics of mitochondrial disorders: two years' experience with whole-exome sequencing at a national paediatric centre. J Transl Med. 2016 Jun 12;14(1):174.

51. Kettwig M, Schubach M, Zimmermann FA, Klinge L, Mayr JA, Biskup S, et al. From ventriculomegaly to severe muscular atrophy: Expansion of the clinical spectrum related to mutations in AIFM1. Mitochondrion. 2015 Mar 1;21:12–8.

52. Sancho P, Sánchez-Monteagudo A, Collado A, Marco-Marín C, Domínguez-González C, Camacho A, et al. A newly distal hereditary motor neuropathy caused by a rare AIFM1 mutation. Neurogenetics. 2017 Dec 1;18(4):245–50.

53. Hu B, Wang M, Castoro R, Simmons M, Dortch R, Yawn R, et al. A novel missense mutation in AIFM1 results in axonal polyneuropathy and misassembly of OXPHOS complexes. European Journal of Neurology. 2017;24(12):1499–506.

54. Wang B, Li X, Wang J, Liu L, Xie Y, Huang S, et al. A novel AIFM1 mutation in a Chinese family with X-linked Charcot–Marie–Tooth disease type 4. Neuromuscular Disorders. 2018 Aug 1;28(8):652–9.

55. Rinaldi C, Grunseich C, Sevrioukova IF, Schindler A, Horkayne-Szakaly I, Lamperti C, et al. Cowchock Syndrome Is Associated with a Mutation in Apoptosis-Inducing Factor. The American Journal of Human Genetics. 2012 Dec;91(6):1095–102.

56. Miyake N, Wolf NI, Cayami FK, Crawford J, Bley A, Bulas D, et al. X-linked hypomyelination with spondylometaphyseal dysplasia (H-SMD) associated with mutations in AIFM1. Neurogenetics. 2017 Dec 1;18(4):185–94.

57. Mierzewska H, Rydzanicz M, Biegański T, Kosinska J, Mierzewska-Schmidt M, Ługowska A, et al. Spondyloepimetaphyseal dysplasia with neurodegeneration associated with AIFM1 mutation - a novel phenotype of the mitochondrial disease. Clinical genetics. 2017 Jan 1;91(1):30–7.

58. Zong L, Guan J, Ealy M, Zhang Q, Wang D, Wang H, et al. Mutations in apoptosis-inducing factor cause X-linked recessive auditory neuropathy spectrum disorder. Journal of Medical Genetics. 2015 Aug 1;52(8):523–31.

59. Sevrioukova IF. Structure/Function Relations in AIFM1 Variants Associated with Neurodegenerative Disorders. Journal of Molecular Biology. 2016 Sep 11;428(18):3650–65.

60. Briston T, Stephen JM, Thomas LW, Esposito C, Chung YL, Syafruddin SE, et al. VHL-Mediated Regulation of CHCHD4 and Mitochondrial Function. Frontiers in Oncology [Internet]. 2018 [cited 2023 Sep 26];8. Available from: https://www.frontiersin.org/articles/10.3389/fonc.2018.00388

61. Zhuang J, Wang P yuan, Huang X, Chen X, Kang JG, Hwang PM. Mitochondrial disulfide relay mediates translocation of p53 and partitions its subcellular activity. Proceedings of the National Academy of Sciences. 2013 Oct 22;110(43):17356–61.

62. Yang J, Staples O, Thomas LW, Briston T, Robson M, Poon E, et al. Human CHCHD4 mitochondrial proteins regulate cellular oxygen consumption rate and metabolism and provide a critical role in hypoxia signaling and tumor progression. J Clin Invest. 2012 Feb 1;122(2):600–11.

63. Thomas LW, Esposito C, Stephen JM, Costa ASH, Frezza C, Blacker TS, et al. CHCHD4 regulates tumour proliferation and EMT-related phenotypes, through respiratory chain-mediated metabolism. Cancer Metab. 2019 Jul 16;7(1):7.

64. Jerabek-Willemsen M, André T, Wanner R, Roth HM, Duhr S, Baaske P, et al. MicroScale Thermophoresis: Interaction analysis and beyond. Journal of Molecular Structure. 2014 Dec 5;1077:101–13.

65. Forneris F, Orru R, Bonivento D, Chiarelli LR, Mattevi A. ThermoFAD, a Thermofluor®-adapted flavin ad hoc detection system for protein folding and ligand binding. The FEBS Journal. 2009;276(10):2833–40.

66. Velázquez-Campoy A, Ohtaka H, Nezami A, Muzammil S, Freire E. Isothermal Titration Calorimetry. Current Protocols in Cell Biology. 2004;23(1):17.8.1-17.8.24.

67. Mirdita M, Schütze K, Moriwaki Y, Heo L, Ovchinnikov S, Steinegger M. ColabFold: making protein folding accessible to all. Nat Methods. 2022 Jun;19(6):679–82.

68. Vonrhein C, Flensburg C, Keller P, Sharff A, Smart O, Paciorek W, et al. Data processing and analysis with the autoPROC toolbox. urn:issn:0907-4449. 2011 Mar 18;67(4):293–302.

69. Emsley P, Lohkamp B, Scott WG, Cowtan K. Features and development of Coot. Acta crystallographica Section D, Biological crystallography. 2010;66(Pt 4):486–501.

70. Winn MD, Ballard CC, Cowtan KD, Dodson EJ, Emsley P, Evans PR, et al. Overview of the CCP4 suite and current developments. Acta crystallographica Section D, Biological crystallography. 2011 Apr;67(Pt 4):235–42.

71. Murshudov GN, Skubák P, Lebedev AA, Pannu NS, Steiner RA, Nicholls RA, et al. REFMAC5 for the refinement of macromolecular crystal structures. Acta crystallographica Section D, Biological crystallography. 2011 Apr;67(Pt 4):355–67.

72. Adams PD, Afonine P V., Bunkóczi G, Chen VB, Davis IW, Echols N, et al. PHENIX: a comprehensive Python-based system for macromolecular structure solution. Acta crystallographica Section D, Biological crystallography. 2010;66(Pt 2):213–21.

73. Blanc E, Roversi P, Vonrhein C, Flensburg C, Lea SM, Bricogne G. Refinement of severely incomplete structures with maximum likelihood in BUSTER-TNT. Acta crystallographica Section D, Biological crystallography. 2004 Dec;60(Pt 12 Pt 1):2210–21.

Manuscripts

Introduction to paper 1

CHCHD4 binding affects the active site of apoptosis inducing factor (AIF): structural determinants of the allosteric regulation.

In this work we characterised the complex formed by the Apoptosis Inducing Factor (AIF) and CHCHD4, to clarify the physiological role of AIF inside mitochondria. We obtained the crystal structure of AIF in complex with the N-terminal portion of CHCHD4 and NAD^+, validated by mass spectrometry analysis on cross-linked complex and mutagenesis experiments on AIF. Structural data integrated with biochemical and biophysical techniques allowed the determination of important features about the interaction.

I optimised the expression and purification protocols to produce the recombinant CHCHD4. I performed the spectrophotometric analyses to study the temperature-dependent effect of CHCHD4 peptide binding on AIF-bound FAD prosthetic group, in the presence of NAD^+. I also obtained the cross-linked complex between AIF and CHCHD4, then used for mass spectrometry analysis, and I built the model of the complex with AlphaFold. I performed crystallisation trials which allowed the structural determination of the complex between AIF and CHCHD4 peptide and I solved and analysed the crystal structure. Finally, I was responsible for mutagenesis experiments on AIF and its biophysical characterization (ThermoFAD, MST, cross-linking) in presence of CHCHD4, to validate the binding site.

Introduction to paper 2

Stabilization of the retromer complex: analysis of novel binding sites of bis-1,3-phenyl guanylhydrazone 2a to the VPS29/VPS35 interface.

The subject of this work is the determination of the binding site of bis-1,3-phenyl guanylhydrazone 2a compound on the retromer complex. The compound was selected for its ability to stabilise the complex in the contest of amyotrophic lateral sclerosis therapy. A combined approach of X-ray crystallography and molecular dynamic simulations allowed the identification of a novel binding site at the interface between VPS29 and VPS35, as a promising target for optimised stabilisers of the retromer complex.

I contributed to this work during my PhD, as a side project, developing the production protocols of the recombinant VPS29-VPS35 short2 complex. I also obtained several diffracting crystals of the complex in presence of the compound, through which it was possible to identify new binding sites.